



1 **Declines and peaks in NO<sub>2</sub> pollution during the multiple waves**  
2 **of the COVID-19 pandemic in the New York metropolitan area**

3

4

5 Maria Tzortziou<sup>1,2</sup>, Charlotte F. Kwong<sup>1</sup>, Daniel Goldberg<sup>3</sup>, Luke Schiferl<sup>4</sup>, Róisín

6 Commane<sup>4,5</sup>, Nader Abuhassan<sup>2,6</sup>, James J. Szykman<sup>7,8</sup>, Lukas C. Valin<sup>8</sup>

7

8

9

10 <sup>1</sup> Center for Discovery and Innovation, Earth & Atmospheric Sciences, City College of New York, New York, NY  
11 10031, USA

12 <sup>2</sup> NASA Goddard Space Flight Center, Greenbelt, MD, 20771, USA

13 <sup>3</sup> Department of Environmental and Occupational Health, George Washington University, Washington, DC, 20052,  
14 USA

15 <sup>4</sup> Lamont Doherty Earth Observatory, Columbia University, Palisades, NY, 10964, USA

16 <sup>5</sup> Department of Earth and Environmental Sciences, Columbia University, New York, NY, 10027, USA

17 <sup>6</sup> Joint Center for Earth Systems Technology, University of Maryland, Baltimore, MD, 21201, USA

18 <sup>7</sup> NASA Langley Research Center, Hampton, VA, 23666, USA

19 <sup>8</sup> US EPA/Office of Research and Development/Center for Environmental Measurement and Modeling, Research  
20 Triangle Park, NC, USA

21

22 *Correspondence to:* Maria Tzortziou ([mtzortziou@ccny.cuny.edu](mailto:mtzortziou@ccny.cuny.edu))

23

24 ORCID

25 MT: 0000-0002-4510-7827

26 CK: 0000-0002-5977-4532

27 DG: 0000-0003-0784-3986

28 LDS: 0000-0002-5047-2490

29 RC: 0000-0003-1373-1550

30 LV: 0000-0002-7314-3868

31



32 **Abstract.** The COVID-19 pandemic created an extreme natural experiment in which sudden changes in human  
33 behavior and economic activity resulted in significant declines in nitrogen oxide (NO<sub>x</sub>) emissions, immediately after  
34 strict lockdowns were imposed. Here we examined the impact of multiple waves and response phases of the  
35 pandemic on nitrogen dioxide (NO<sub>2</sub>) dynamics and the role of meteorology in shaping relative contributions from  
36 different emission sectors to NO<sub>2</sub> pollution in post-pandemic New York City. Long term (> 3.5 years), high  
37 frequency measurements from a network of ground-based Pandora spectrometers were combined with TROPOMI  
38 satellite retrievals, meteorological data, mobility trends, and atmospheric transport model simulations to quantify  
39 changes in NO<sub>2</sub> across the New York metropolitan area. The stringent lockdown measures after the first pandemic  
40 wave resulted in a decline in top-down NO<sub>x</sub> emissions by approx. 30% on top of long-term trends, in agreement  
41 with sector-specific changes in NO<sub>x</sub> emissions. Ground-based measurements showed a sudden drop in total column  
42 NO<sub>2</sub> in spring 2020, by up to 36% in Manhattan and 19-29% in Queens, New Jersey and Connecticut, and a clear  
43 weakening (by 16%) of the typical weekly NO<sub>2</sub> cycle. Extending our analysis to more than a year after the initial  
44 lockdown captured a gradual recovery in NO<sub>2</sub> across the NY/NJ/CT tri-state area in summer and fall 2020, as social  
45 restrictions eased, followed by a second decline in NO<sub>2</sub> coincident with the second wave of the pandemic and  
46 resurgence of lockdown measures in winter 2021. Meteorology was not found to have a strong NO<sub>2</sub> biasing effect  
47 in New York City after the first pandemic wave. Winds, however, were favorable for low NO<sub>2</sub> conditions in  
48 Manhattan during the second wave of the pandemic, resulting in larger column NO<sub>2</sub> declines than expected based on  
49 changes in transportation emissions alone. Meteorology played a key role in shaping the relative contributions from  
50 different emission sectors to NO<sub>2</sub> pollution in the city, with low-speed (< 5 ms<sup>-1</sup>) SW-SE winds enhancing  
51 contributions from the high-emitting power-generation sector in NJ and Queens and driving particularly high NO<sub>2</sub>  
52 pollution episodes in Manhattan, even during – and despite - the stringent early lockdowns. These results have  
53 important implications for air quality management in New York City, and highlight the value of high resolution NO<sub>2</sub>  
54 measurements in assessing the effects of rapid meteorological changes on air quality conditions and the  
55 effectiveness of sector-specific NO<sub>x</sub> emission control strategies.  
56



## 57 1. Introduction

58 The global outbreak of the Coronavirus Disease 2019 (COVID-19) profoundly changed the world. From school closures  
59 to remote work and other physical distancing measures, this crisis changed the way we move within our communities,  
60 potentially with long term implications (Barbieri et al., 2021; Przybyłowski et al., 2021). Altered mobility patterns led to  
61 sudden and significant worldwide decreases in nitrogen oxide (NO<sub>x</sub>) emissions from the transportation sector, as  
62 documented in many studies focusing on air quality changes immediately after the initial lockdowns (e.g., Liu et al.,  
63 2020; Goldberg et al., 2020; Gkatzelis et al., 2021). Yet, the impact of multiple pandemic waves over longer time periods,  
64 and the role of meteorology and sector-specific emissions as key drivers of high NO<sub>x</sub> pollution episodes that occurred in  
65 major cities such as New York - even during, and despite, the most stringent early lockdown periods - remain largely  
66 unknown, driving this study.

67  
68 New York City, the most populous and most densely populated city in the United States, was hit particularly hard by  
69 the pandemic. By late-March 2020, the tri-state region of New York (NY), New Jersey (NJ) and Connecticut (CT)  
70 declared a disaster emergency and issued stay-at-home restrictions in response to COVID-19. Almost 8 million New  
71 Yorkers sheltered-in-place, while roughly 5% of New York City residents (about 420,000 people) left the city between  
72 March and May (Quealy, 2020; Bounds, 2020). The largest decrease in residential population occurred in Manhattan—  
73 with more than 30% reduction in relatively wealthy neighborhoods including Upper West and Upper East Side—while  
74 the rest of the city saw comparably modest losses (Quealy, 2020). The entire New York metropolitan area remained  
75 in lockdown with strict social distancing measures, including school and non-essential business closures, limited  
76 transit services, and suspension of public events and gatherings, for more than two months, from mid-March through  
77 June 2020. Lockdown measures were relaxed and the first phase of reopening began in June with the area progressing  
78 to the final stage of reopening in July. Yet, social distancing measures became strict again, including school closures,  
79 as the city experienced a surge in COVID-19 cases in late fall 2020 that reached a maximum in mid-January 2021  
80 with more reported cases to NYC Department of Health and Mental Hygiene than during the first wave of the  
81 pandemic (Fig. S1). Early studies using satellite data from the Ozone Monitoring Instrument (OMI) and the  
82 Tropospheric Monitoring Instrument (TROPOMI) revealed 31(±14)% and 28(±11)% reduction, respectively, in  
83 nitrogen dioxide (NO<sub>2</sub>) column amount within a 100-km radius of New York City during the three weeks following  
84 the onset of the pandemic compared to the same period in 2019 (Bauwens et al., 2020). Similarly, Goldberg et al.,  
85 (2020) reported a 20% drop in TROPOMI NO<sub>2</sub> within a 0.4° radius of New York between March 13 and April 30,  
86 2020.

87  
88 Emitted to the atmosphere primarily during fossil fuel combustion, nitrogen oxides (NO<sub>x</sub>=NO+NO<sub>2</sub>) are a major  
89 source of air pollution and necessary precursors of tropospheric ozone, impacting climate as well as human and  
90 ecosystem health (Fares et al., 2013; Duan et al., 2019; Lim et al., 2012; Burnett et al., 2004). High NO<sub>2</sub> levels have  
91 been associated with lung irritation and reduced lung function, increased asthma attacks, cardiovascular disorders, as  
92 well as lower birth weight in newborns and increased risk of premature death (U.S. EPA 2016). In addition, through  
93 wet and dry deposition, the atmosphere is a major source of excess nitrogen to many terrestrial and aquatic ecosystems



94 worldwide (Paerl et al., 2002; Pardo et al., 2011). Prior studies have indicated atmospheric deposition accounts for a  
95 third or more of total nitrogen loading in systems such as the Chesapeake Bay and Long Island Sound, with important  
96 implications for soil biogeochemistry, aquatic biology, development of coastal eutrophication, harmful algal blooms,  
97 and hypoxia (e.g., Stacey et al., 2001; Decina et al., 2017; Decina et al., 2020). A combination of strict air quality  
98 regulation policies (e.g., Clean Air Interstate Rule, CAIR, 2009) and technological improvements over the past two  
99 decades has resulted in significant declines in NO<sub>x</sub> emissions over the continental United States (van der A et al.,  
100 2008; Duncan et al., 2016; Krotkov et al., 2016). Satellite Aura/OMI observations have captured an approximately  
101 4% yr<sup>-1</sup> decrease in column NO<sub>2</sub> levels between 2005 and 2015 over the eastern United States (Krotkov et al., 2016)  
102 and a 46% decline in NO<sub>x</sub> emissions has been reported for New York City over the period from 2006 to 2017  
103 (Goldberg et al., 2019a). Despite these improvements, air pollution continues to be the single biggest environmental  
104 health risk in the United States and globally today (Burnett et al., 2018; Thakrar et al., 2020; WHO 2019). With  
105 significant NO<sub>x</sub> emissions from various sectors (e.g., transportation, energy, industrial), the New York metropolitan  
106 area experiences among the highest national NO<sub>2</sub> levels (Herman et al., 2018) and has the worst nonattainment record  
107 of ozone in eastern North America (based on the EPA 2015 standard) (Karambelas et al., 2020).

108

109 Restrictions on human and economic activities, particularly reductions in transportation emissions due to the COVID-  
110 19 stay-at-home orders, provide a unique opportunity to assess the importance of different sources of air pollution in  
111 New York City and how further sector-specific NO<sub>x</sub> emission reductions may impact nitrogen pollution in this major  
112 urban center. The overarching objective of this study was to examine how NO<sub>2</sub> dynamics changed in the New York  
113 metropolitan area during the multiple phases of the pandemic and across regions experiencing different shifts in  
114 mobility patterns. Ground-based measurements conducted over a period of 3.5 years (2017-2021) allowed us to  
115 capture inter-annual variability, impacts of meteorology, and changes in air quality as human behavior changed during  
116 the multiple pandemic waves and as vehicle traffic started to return to near pre-pandemic levels a year after the initial  
117 lockdown. Combining these high-frequency observations with model simulations and satellite imagery uniquely  
118 captured NO<sub>2</sub> dynamics across multiple scales and highlighted the impact of COVID-19 restrictions not only on NO<sub>2</sub>  
119 column amounts but also on NO<sub>2</sub> spatiotemporal behavior, including seasonal and weekly cycles.

120

121 Meteorological factors have a significant impact on atmospheric chemistry as well as transport, transformation, and  
122 dispersion of air pollutants (Xu et al., 2011; Banta et al., 2011; Goldberg et al., 2020). Elucidating the role of  
123 meteorology is thus important in assessments of COVID-19 impacts on urban air quality (Gkatzelis et al., 2021).  
124 Seasonality and local meteorology were previously reported to drive NO<sub>2</sub> changes in New York City as large as a  
125 factor of two over the course of a year (Goldberg et al., 2020). Although meteorological patterns were especially  
126 favorable for low NO<sub>2</sub> in much of the United States in spring 2020, varying meteorological conditions in New York  
127 City were not found to have a biasing effect in TROPOMI estimates of NO<sub>2</sub> declines during the initial lockdown  
128 period (Goldberg et al., 2020). Because our study extended over a longer time-period, we explicitly investigated how  
129 weather conditions may have impacted observed changes in NO<sub>2</sub> pollution and the relative contribution of different  
130 NO<sub>x</sub> emissions sectors (i.e., energy versus transportation) during the multiple phases of the pandemic.



131 **2. Methods**

132 **2.1 Ground-based measurements of column NO<sub>2</sub> dynamics**

133 To assess the impact of COVID-19 restrictions on NO<sub>2</sub> spatiotemporal behavior we used high-frequency  
 134 measurements of total column NO<sub>2</sub> (TCNO<sub>2</sub>) from the ground-based Pandonia Global Network (PGN,  
 135 <https://www.pandonia-global-network.org/>). Sponsored by the National Aeronautics and Space Administration (NASA)  
 136 and the European Space Agency (ESA), PGN focuses on providing long-term, real-time and verified QA/QC data on  
 137 air quality and atmospheric composition from a network of standardized and calibrated Pandora spectrometer  
 138 instruments (PSIs, Herman et al., 2019). The PGN global network serves as a validation resource for UV-visible  
 139 satellite sensors on low-earth and geostationary orbit, and recent studies have included Pandora measurements for  
 140 ground-based validation of TROPOMI NO<sub>2</sub> measurements near New York City and Long Island Sound (Judd et al.,  
 141 2020; Verhoelst et al., 2021). In the New York metropolitan area, PGN sites include Manhattan, NY (PSI #135),  
 142 Queens, NY (PSIs #55, #140), New Brunswick, NJ (PSIs #56, #69), and New Haven, CT (PSIs #20, #64) (Table 1,  
 143 Fig. 1). PSI #135 in Upper West Manhattan, NY, has the longest data record (since Dec 2017) among these instruments  
 144 and is located on the Advanced Science Research Center (ASRC) Rooftop Observatory at the City College of New  
 145 York campus, an intensive urban air-quality monitoring site. The Pandora sensor in Queens, NY, is located at the  
 146 CUNY Queens College, a New York Department of Environmental Conservation (NYDEC) Air Toxics and NCore  
 147

Pandora name, #, location (Principal Investigator)	Temporal range of data		TCNO <sub>2</sub> (in DU)							
			Apr-May		June-Aug		Sept-Nov		Dec-Feb	
			Pre-	Post-	Pre-	Post-	Pre-	Post-	Pre-	Post-
Manhattan, NY PSI #135 40.8153°, -73.9505°	12/2017 - Present	mean stdev max	0.61 0.34 3.11	0.39 0.25 3.25	0.59 0.35 3.77	0.44 0.24 2.09	0.59 0.38 2.94	0.46 0.27 1.89	0.71 0.45 3.13	0.48 0.30 2.05
(M. Tzortziou)		<b>change</b>		<b>-36%</b>	<b>-25%</b>		<b>-22%</b>		<b>-32%</b>	
Queens, NY PSI #140, #55 40.7361°, -73.8215°	5/2018 - Present	mean stdev max	0.61 0.35 3.42	0.48 0.21 3.60	0.54 0.28 2.74	0.51 0.19 1.54	0.57 0.33 3.36	0.51 0.22 2.34	0.73 0.40 3.04	0.70 0.38 2.81
(J. Szykman)		<b>change</b>		<b>-21%</b>	<b>-6%</b>		<b>-11%</b>		<b>-4%</b>	
New Brunswick, NJ* PSI #56, #69 40.4622°, -74.4294°	5/2018 - 1/2021	mean stdev max	0.32 0.15 1.46	0.26 0.18 2.06	0.29 0.15 1.98	0.28 0.20 2.42	0.34 0.24x 2.55	0.30 0.21 4.59	0.42 0.31 2.72	0.26 0.10 0.53
(J. Szykman)		<b>change</b>		<b>-19%</b>	<b>-3%</b>		<b>-12%</b>		<b>-38%</b>	
New Haven, CT PSI #20, #64 41.3014°, -72.9029°	5/2018 - Present	mean stdev max	0.38 0.11 0.75	0.27 0.08 0.78	0.34 0.09 0.77	0.29 0.08 0.83	0.34 0.15 1.71	0.29 0.13 1.13	0.36 0.17 1.37	0.33 0.18 1.83
(J. Szykman)		<b>change</b>		<b>-29%</b>	<b>-15%</b>		<b>-15%</b>		<b>-8%</b>	

148  
 149  
 150

\* The Dec – Feb period for New Brunswick contains 16 days of data in December 2020, 1 day of data in January 2021, and no data in February 2021.

151 **Table 1: Pandora sites (including names of Local Principal Investigator (PI)), and mean, standard deviation (stdev) and**  
 152 **maximum (max) total column NO<sub>2</sub> (TCNO<sub>2</sub>) amounts (based on half-hour averages) measured pre- and post- the COVID-**  
 153 **19 lockdown in New York.**

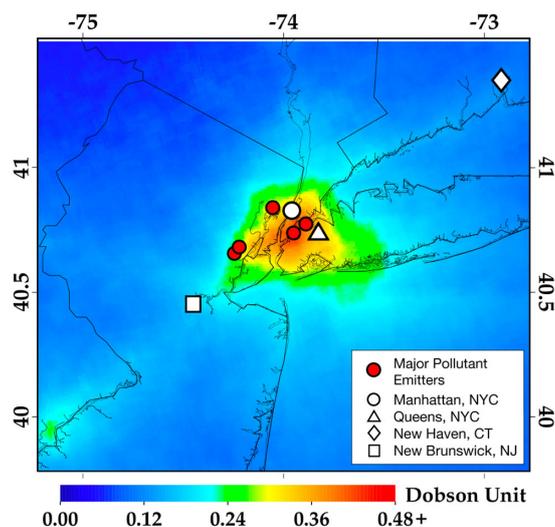


**Figure 1:** Map of study area, indicating location of Pandora sensors (white symbols) in Manhattan NY, Queens NY, New Brunswick NJ, and New Haven CT, overlaid with mean 2019 annual total column NO<sub>2</sub> from TROPOMI (in DU). Major pollutant emitters (red circles) in the area are included, specifically the PSEG Bergen Generating Station in Ridgefield, and the Linden Generating Station, the Linden Cogeneration Facility, and the Phillips 66 Bayway Refinery (major emission sources in NJ), and the Astoria and Ravenswood Generating Stations in Queens, NY (among the largest greenhouse gas polluters in the state of NY in 2018 and 2019).

154 monitoring site within a dense residential neighborhood and near several major roadways. The Pandora in New Haven,  
155 CT, is located at the Connecticut Department of Energy and Environmental Protection (CTDEEP) Photochemical  
156 Assessment Monitoring Station (PAMS) in Criscuolo Park, at the confluence of the Mill and Quinnipiac Rivers  
157 surrounded by a residential neighborhood near the elevated intersection of three major highways and industrial  
158 activities across the rivers. The New Jersey Department of Environmental Protection (NJDEP) Photochemical  
159 Assessment Monitoring Station (PAMS) in New Brunswick, NJ, includes a Pandora sensor located on the roof of the  
160 Rutgers (NJDEP) research shelter dedicated to atmospheric research, on a university research farm in a suburban  
161 neighborhood and approximately 20 km from the coast.

162

163 Pandora is a sun/sky/lunar passive UV/Visible spectrometer system, driven by a highly accurate sun tracker that points  
164 an optical head at the sun and transmits the received light to an Avantes low stray light CCD spectrometer (spectral  
165 range: 280-525 nm; spectral resolution: 0.6 nm with 4 times oversampling) through a fiber optic cable (Herman et al.,  
166 2019; Tzortziou et al., 2014). The spectrometer is temperature stabilized at 20°C inside a weather resistant container.  
167 Trace gas abundances along the light path are determined using differential optical absorption spectroscopy (DOAS).  
168 The system can operate in both direct-sun and sky-scan mode for retrievals of O<sub>3</sub>, NO<sub>2</sub>, SO<sub>2</sub> and CH<sub>2</sub>O total columns,  
169 tropospheric columns, and information on vertical profile (Tzortziou et al., 2018; Herman et al., 2018; Spinei et al.,  
170 2018), and is an enhanced monitoring instrument for characterizing upper air pollutants under the U.S. EPA PAMS  
171 program (Szykman et al., 2019). The estimated TCNO<sub>2</sub> error in Pandora retrievals is approximately 0.05 DU (1 DU



172 =  $2.69 \times 10^{16}$  molecules  $\text{cm}^{-2}$ ) (Herman et al., 2019). Pandora data were filtered here for normalized root-mean square  
173 of weighted spectral fitting residuals less than 0.05, uncertainty in  $\text{NO}_2$  retrievals less than 0.05 DU, and  $\text{TCNO}_2 > 0$ .

## 174 2.2 TROPOMI satellite retrievals

175 Jointly developed by the Netherlands and ESA, TROPOMI is an air quality monitoring sensor onboard the sun-  
176 synchronous Copernicus Sentinel-5 Precursor satellite, launched on 13 October 2017 (Veeffkind et al., 2012). On a  
177 low-earth (825 km) orbit, Sentinel-5P has a daily equator overpass time of approximately 13:30 local time and global  
178 daily coverage. TROPOMI has a spatial resolution of 7.2 km (5.6 km as of 6 August 2019) along-track by 3.6 km  
179 across-track at nadir, a significant improvement compared to its predecessors OMI (Ozone Monitoring Instrument)  
180 and SCIAMACHY (SCanning Imaging Absorption spectroMeter for Atmospheric Cartography). Several spectral  
181 bands in the ultraviolet to shortwave-infrared (270–2385 nm) and a spectral resolution between 0.25 and 1 nm, allow  
182 observations of cloud, aerosol properties, and key atmospheric trace gases including  $\text{O}_3$ ,  $\text{NO}_2$ , CO,  $\text{SO}_2$ ,  $\text{CH}_4$  and  
183  $\text{CH}_2\text{O}$  (Veeffkind et al., 2012).  $\text{NO}_2$  retrievals from TROPOMI are based on measurements in the 405–465 nm spectral  
184 window. Using a DOAS technique, similar to the Pandora instrument, the top-of-atmosphere spectral radiances are  
185 converted into slant column amounts of  $\text{NO}_2$  between the sensor and the Earth's surface (Boersma et al., 2018). In two  
186 additional steps, subtraction of the stratospheric component and incorporation of an air mass factor, the slant column  
187 quantity is converted into a tropospheric vertical column content (Beirle et al., 2019; Dix et al., 2020; Goldberg et al.,  
188 2019b; Griffin et al., 2019; Ialongo et al., 2020; Reuter et al., 2019; Zhao et al., 2020). For this analysis, we used the  
189 operational “off-line” TROPOMI  $\text{NO}_2$  data set, Version 1.02 between 30 April 2018 – 19 March 2019 and Version  
190 1.03 20 March 2019 – 28 November 2020. We do not continue the TROPOMI analysis beyond 28 November 2020  
191 due to a significant change in the algorithm (to version 1.04) on 29 November 2020. TROPOMI data are filtered using  
192 a quality assurance flag (QA), in which pixels with QA values greater than 0.75 are utilized; no other filter has been  
193 applied. Validation of TROPOMI  $\text{NO}_2$  V1.2 tropospheric columns over the New York City metropolitan area indicate  
194 columns are biased low, varying 19–33% (Judd et al., 2020).

## 195 2.3 Satellite-derived $\text{NO}_x$ emissions

196 We used an inverse statistical modeling technique (Goldberg et al., 2019b; Laughner & Cohen 2019) to derive the  
197 New York City  $\text{NO}_x$  emission rates from a combination of TROPOMI satellite data and re-analysis meteorology. This  
198 method accounts for daily changes in temperature, sun angle, wind speed and wind direction by calculating a  
199 spatiotemporally specific  $\text{NO}_2$  lifetime. In brief, all  $\text{NO}_2$  satellite data over New York City were compiled and rotated  
200 based on the daily-observed wind direction, so that the oversampled plume is decaying in a single direction. We used  
201 the closest gridded value without interpolation of the 100-m (above the surface) horizontal wind speed and direction  
202 from the ERA5 re-analysis dataset (Hersbach et al., 2020) generated at  $0.25^\circ \times 0.25^\circ$ . Once all daily plumes were  
203 rotated to be aligned as an effective horizontal plume and averaged together during a 5-month warm season period  
204 (May–Sept; usually  $\sim 75$  snapshots), we integrated  $\pm 0.5^\circ$  along the y-axis about the x-axis to compute a one-



205 dimensional line density in units of mass per distance. The line densities, which are parallel to the wind direction,  
206 peak near the primary  $\text{NO}_x$  emissions source and gradually decay downwind from a combination of atmospheric  
207 dispersion, chemical transformation, and deposition. The line densities were fit to a statistical exponentially modified  
208 Gaussian (EMG) model (Beirle et al., 2011; de Foy et al., 2014; Valin et al., 2013; Verstraeten et al., 2018). The five  
209 fitted parameters of the statistical fit are the  $\text{NO}_2$  background,  $\text{NO}_2$  mass perturbed above the background threshold  
210 (burden), decay distance, horizontal location of apparent source (ideally at the origin), and sigma of the Gaussian  
211 plume. The  $\text{NO}_x$  emissions rate from the source can be calculated from the  $\text{NO}_2$  burden, decay distance, and  $\text{NO}_x/\text{NO}_2$   
212 ratio, which previous work has shown to be 1.33 (Beirle et al., 2011). After accounting for a systematic low bias of  
213 TROPOMI in polluted areas (Judd et al., 2020; Verhoelst et al., 2021), the  $\text{NO}_x$  emissions compare well with known  
214 emissions from power plants (Goldberg et al., 2019b). For this project, we do not correct for TROPOMI low bias, but  
215 instead assume the low bias is consistent between years and calculate changes between years. A full description of the  
216 method can be found in Goldberg et al. (2019a; b).

#### 217 **2.4 STILT model simulations**

218 We used STILT, the Stochastic Time-Inverted Lagrangian Transport model, to calculate the surface influence and  
219 contributions from different sources of  $\text{NO}_2$  pollution to the city. STILT is a Lagrangian particle dispersion model, in  
220 this case driven by NOAA High-Resolution Rapid Refresh (HRRR) meteorology at 3 km horizontal resolution, that  
221 follows the trajectory of 500 air parcels released from the receptor (measurement site) position backward in time over  
222 the previous 24 hours. The motion of each parcel is determined by both advection by the large-scale wind fields and  
223 random turbulent motion, independent of the other parcels. The proportion of parcels residing in the lower half of the  
224 planetary boundary layer determines the influence of surface fluxes on the measured mole fractions. This surface  
225 influence is tracked in time and space, which allows for the calculation of a two-dimensional footprint at hourly  
226 intervals over the travel period and spatial domain of the particles. The unit of surface influence is defined as the  
227 response of each receptor concentration measurement to a unit emission of a trace gas at each grid square (e.g., ppb  
228  $(\mu\text{mol m}^{-2}\text{s}^{-1})^{-1}$ ). In this study, we ran hourly STILT simulations for the 10 hours surrounding daily peak  $\text{NO}_2$ , for cases  
229 of particularly high column  $\text{NO}_2$  amounts ( $> 1.8$  DU, more than three times the average of pre-pandemic levels)  
230 measured at the Manhattan and Queens Pandora sites during the COVID-19 lockdown in April 2020 and after the  
231 shutdown in October 2020. Simulated particles originated at the elevation of the Pandora instruments. We also  
232 performed simulations for one low  $\text{NO}_2$  case in April 2020 for comparison. The STILT footprints were multiplied by  
233 2015 annual gridded maps of  $\text{NO}_x$  emissions  $(\mu\text{mol m}^{-2}\text{s}^{-1})$  at  $0.1^\circ$  horizontal resolution from the Emissions Database  
234 for Global Atmospheric Research (EDGAR) v5.0, which combine atmospheric pollutant data categorized by  
235 anthropogenic emissions sector (e.g., power, manufacturing, transportation), to predict the  $\text{NO}_2$  concentration  
236 enhancement (ppb) that would be expected for each observed hour.



## 237 2.5 Meteorological Data

238 Wind speed and direction data from the ERA5 Model (Copernicus Climate Change Service (C3S), 2017) were used  
239 to examine the impact of meteorology on TROPOMI retrieved NO<sub>2</sub> column amounts. To downscale the 0.25° × 0.25°  
240 grid ERA5 reanalysis, we spatially interpolate daily averaged winds to 0.01° × 0.01° using bilinear interpolation  
241 (Goldberg et al., 2020). The average 100-m winds during 16–21 UTC (i.e., approximately the TROPOMI overpass  
242 time over North America) were used in our analysis. To assess impacts of meteorology on ground-based measurements  
243 of TCNO<sub>2</sub> from the Manhattan Pandora PSI#135, we used in situ measurements of wind speed and wind direction  
244 (measured at a resolution of 0.01 m/s and 1°, respectively) collected by a collocated ATMOS 41 All-In-One weather  
245 station on a 15-minute timescale.

## 246 2.6 Calculation of change in NO<sub>2</sub> column amounts

247 Change in NO<sub>2</sub> column amounts was estimated by comparing post-lockdown TROPOMI and Pandora measurements  
248 to the same timeframe in 2018-2019, to account for seasonality and interannual variability (Goldberg et al., 2020;  
249 Bauwens et al., 2020). The impact of meteorology on these estimates was explicitly quantified using ERA5 and in situ  
250 meteorological data. We estimated changes in NO<sub>2</sub> over the different phases of the pandemic in New York City (i)  
251 immediately following the initial lockdown in April-May 2020, (ii) as restrictions gradually eased in June-August  
252 2020, (iii) during the re-opening phase in September-November 2020, (iv) as restriction became strict again in  
253 December 2020-February 2021 due to the second wave of the pandemic, and (v) in March-April 2021, one year after  
254 the initial lockdown. Pandora data were first averaged in half-hour bins to eliminate bias towards times of day with  
255 more data, then averaged on weekly, monthly, and seasonal time scales. To examine weekly cycles from satellite  
256 observations, TROPOMI data were averaged over longer timescales (April-November), due to the lower temporal  
257 resolution and impacts of clouds on satellite retrievals. All computed means for seasonal and weekly cycles were  
258 calculated with 95% confidence intervals using a two-tailed single sample t-test. While NO<sub>2</sub> data is non-normally  
259 distributed, all sample sizes are large (n > 100), and statistics (e.g., p-values) were also calculated using the  
260 nonparametric Mann-Whitney and Kruskal Wallis tests which confirmed the validity of t-test results.

## 261 2.7 Changes in mobility patterns

262 To examine changes in mobility patterns, we looked at sector-specific mobility indices provided by Apple (Forster et  
263 al., 2020) and traffic counts from the Metropolitan Transport Authority (MTA) day-by-day transit data, focusing on  
264 bridge and tunnel ridership to represent passenger vehicles (buses, motorcycles, cars, trucks) (NY MTA). Apple  
265 mobility data (accessed on 4 June 2021) tracked mobile phone movements and compared post-COVID-19 data with  
266 the average on February 13, 2020 (Forster et al., 2020). For MTA data (accessed on 4 June 2021), bridge and tunnel  
267 traffic was quantified from E-ZPass and cash toll collection, and percent (%) changes in ridership were calculated  
268 through comparison to traffic on the pre-COVID equivalent day in the previous year.



## 269 3. Results and Discussion

### 270 3.1. Changes in NO<sub>2</sub> column amounts and spatiotemporal dynamics

271 Satellite imagery from TROPOMI captured significant post-shutdown NO<sub>2</sub> reductions in the New York metropolitan  
272 area, particularly during the first three months after the initial lockdowns (Fig. 2). As MTA bridge and tunnel traffic  
273 plummeted by up to 80% in April 2020 (Fig. S2), TCNO<sub>2</sub> over a 50 x 50 km area around Manhattan dropped by 32%  
274 in March-May 2020 compared to the same period in 2018-2019 (Fig. 2, left panel). Smaller declines (< 30%) were  
275 found in the surrounding areas of NJ, upstate NY, and CT. These results are consistent with Bauwens et al., (2020)  
276 reporting a decline in TROPOMI NO<sub>2</sub> column by 28(±11)% within a 100-km radius around New York City during  
277 the three weeks following the onset of the pandemic compared to the same period in 2019. By June-August 2020, total  
278 NO<sub>2</sub> columns—lower during summer due to increased photochemical loss—rose closer to pre-pandemic levels, with  
279 approx. 15% decline over New York City and even smaller changes (<10%) in western NJ, CT, and eastern Long  
280 Island (Fig. 2, mid panel). This recovery in NO<sub>2</sub> coincided with the city of New York commencing the first phase of  
281 its reopening plan in June 2020 and gradually relaxing lockdown measures, including the opening of restaurants  
282 (outdoor dining) and some workplaces. Daily traffic on New York City bridges and tunnels increased to 22% lower  
283 than baseline in summer 2020 (Fig. S2). This trend continued in fall 2020, with TCNO<sub>2</sub> showing 13% drop over New  
284 York City and smaller declines over more rural areas in northern NJ and eastern Long Island (Fig. 2, right panel).

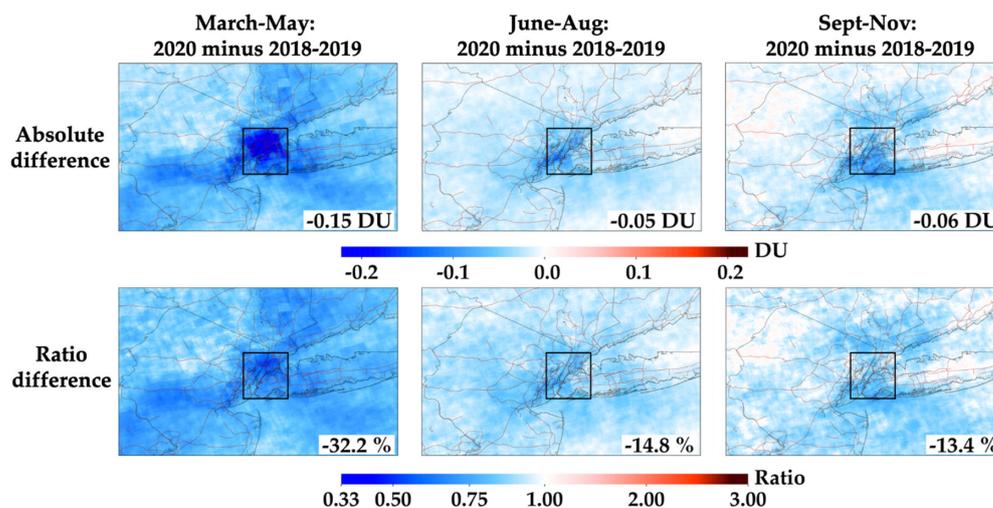
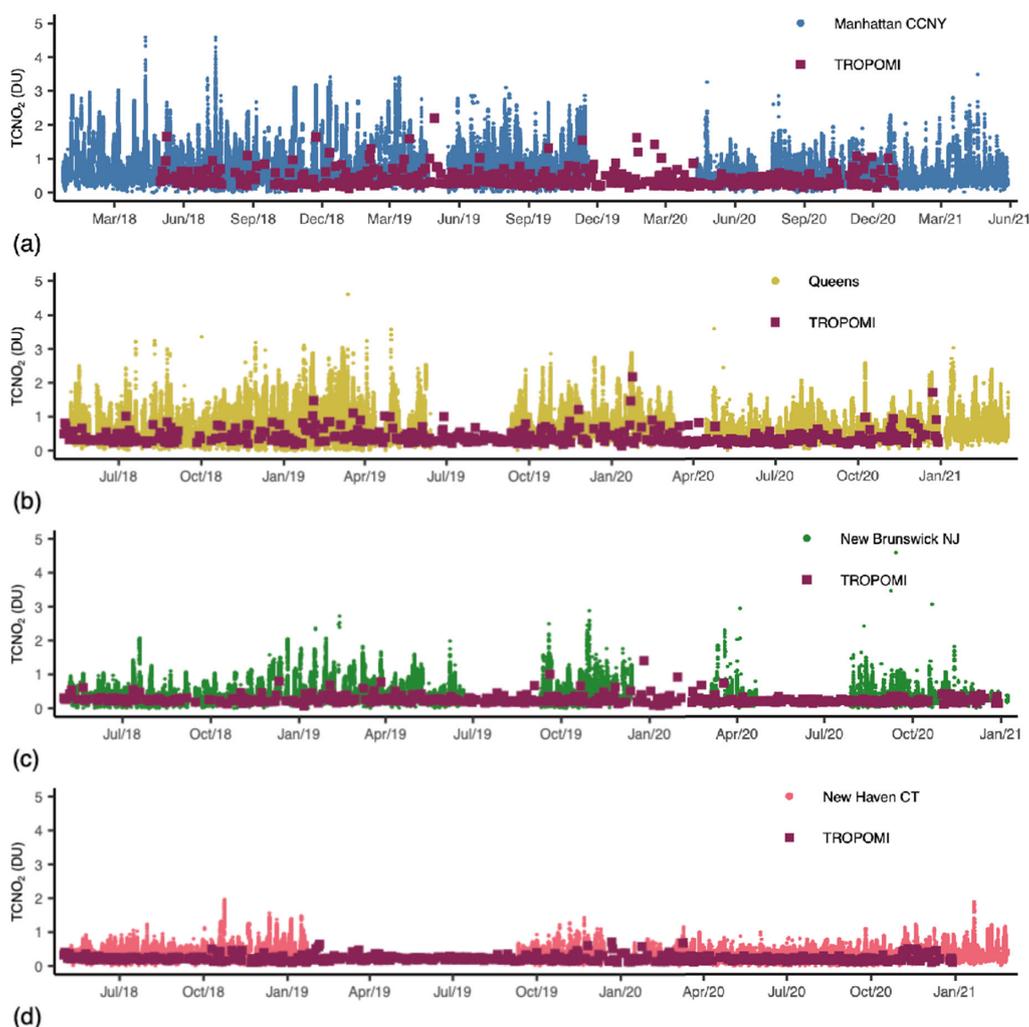


Figure 2: TROPOMI total vertical column NO<sub>2</sub> differences between 2018-2019 and 2020, over the New York metropolitan area. Results are shown for 13 March through May (left panels), June through August (middle panels) and September through November (right panel). Upper panels show the absolute difference between the 3-month period in 2018-2019 and 2020 in Dobson units. Bottom panels show the ratio between the 3-month period in 2018-2019 and 2020. Values denoted in bottom right of each panel are area-averaged difference within a 50 x 50km area around Manhattan (black box). 13 March – 29 April 2019 data are double counted in the March through May 2018 – 2019 period due to unavailable data in the 13 March – 29 April 2018 timeframe.



285

286 These abrupt spatiotemporal changes in TCNO<sub>2</sub> detected by TROPOMI were remarkably consistent with the higher  
287 resolution measurements from the ground-based Pandora network. Prior to lockdown, TCNO<sub>2</sub> in Manhattan and  
288 Queens, NY, was characterized by high variability, often surpassing 2 DU (Fig. 3). NO<sub>2</sub> total columns in New  
289 Brunswick, NJ, and New Haven, CT, were overall considerably lower than measurements in New York City, in  
290 agreement with pre-pandemic TROPOMI retrievals (Table 1, Figs. 1, 3). Across all sites, pre-pandemic TCNO<sub>2</sub>  
291 showed a clear seasonal cycle typical of Northern Hemisphere mid-latitude locations, with maxima occurring during  
292 the winter (Figs. 3, 4) due largely to increased fossil fuels for domestic heating, the longer tropospheric NO<sub>2</sub> lifetime



**Figure 3:** Long term (December 2017- February 2021, May 2021 in Manhattan only) data record of TCNO<sub>2</sub> (in DU) measured by Pandoras in (a) Upper West Side Manhattan (blue circles), (b) Queens (yellow circles), (c) New Brunswick NJ (green circles) and (d) New Haven CT (pink circles). Total column TROPOMI overpass data at locations of the Pandora instruments is also shown (red squares). No data averaging was performed on Pandora or TROPOMI values.



293 at colder temperatures, less light availability, and a shallower and more stable planetary boundary layer (A et al., 2008;  
294 Semple et al., 2012). Post-shutdown, all Pandora sensors measured a significant drop in TCNO<sub>2</sub>. In the two months  
295 following the initial lockdown, TCNO<sub>2</sub> in Manhattan decreased by 36% compared to pre-pandemic levels, with  
296 smaller declines, 21%, 19% and 29% respectively, in Queens, New Brunswick, and New Haven (Table 1). Variability  
297 in TCNO<sub>2</sub> (Table 1) also decreased, indicating a reduction in the magnitude of high NO<sub>2</sub> pollution episodes. As social  
298 distancing restrictions gradually started to ease in June, TCNO<sub>2</sub> in Manhattan started to slowly recover, reaching 25%  
299 lower than the pre-pandemic seasonal mean in summer and 22% lower in fall 2020. NO<sub>2</sub> rose even closer to pre-  
300 pandemic levels in Queens, New Brunswick, and New Haven, showing less than 15% decline in summer and fall 2020  
301 (Table 1), consistent with our TROPOMI results. TCNO<sub>2</sub> in Manhattan, however, dropped again significantly below  
302 pre-pandemic levels during the second wave of the pandemic in late 2020 (Table 1, Fig. 4). The decline in TCNO<sub>2</sub>  
303 reached 39% in January 2021, consistent with both a decline in mobility (i.e., re-closing of businesses and transition  
304 from in-person to online learning in many schools in the area; Fig. S1) as well as favorable meteorological conditions  
305 for low NO<sub>2</sub> (discussed in section 3.4). As restrictions eased again, NO<sub>2</sub> levels rebounded to 11% and 21% below pre-  
306 pandemic levels in April and May 2021, respectively, more than a year after the COVID-19 outbreak in the U.S.  
307 (Table 1, Fig. 4).

308

309 These changes resulted in a departure from typical seasonal NO<sub>2</sub> behavior, maximum in winter and minimum in  
310 summer, with instead a maximum in monthly mean TCNO<sub>2</sub> in July 2020 and two minima tightly linked to the two  
311 pandemic waves in May 2020 and January 2021 (Fig. 4). In agreement with Gkatzelis et al. (2021), the NO<sub>2</sub> decrease  
312 closely followed changes in the stringency of lockdown measures and particularly decreases in traffic, further  
313 confirming the importance of the transportation sector as a source of NO<sub>x</sub> pollution in Manhattan. Still, as discussed  
314 in the next section, other emission sectors also contributed significantly to the observed spatiotemporal changes in  
315 NO<sub>2</sub> pollution over the New York metropolitan area during the multiple waves of the pandemic.

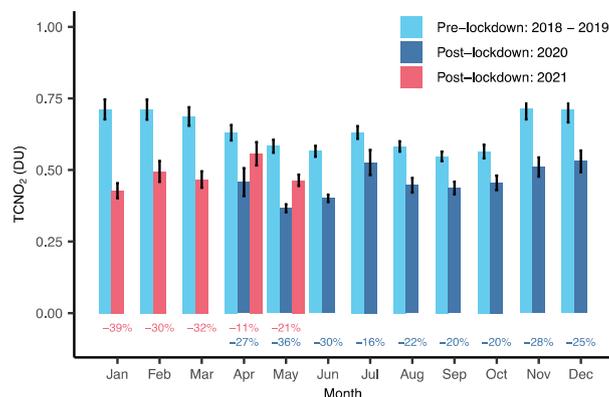


**Figure 4: Monthly mean seasonal cycle of TCNO<sub>2</sub> in Upper West Manhattan pre-lockdown (Dec 2017-Dec 2019, cyan) and post-lockdown (Apr 2020-Dec 2020, blue and January-May 2021, red), as measured by PSI #135 (30 min averaged data; 95% confidence intervals indicated by error bars; data not available during Jan-Mar 2020). The percent (%) change is also shown below each bar.**



### 316 3.2. Impacts of COVID-19 measures on NO<sub>x</sub> emissions

317 While meteorology plays a significant role in air pollution levels, our estimates of top-down NO<sub>x</sub> emissions from  
318 TROPOMI indicate that sudden reductions in NO<sub>x</sub> emissions due to COVID-19 measures were the dominant factor  
319 driving the observed NO<sub>2</sub> decline in New York City during the first wave of the pandemic (Fig. 5). Five-month (May  
320 to September) averaged top-down NO<sub>x</sub> emissions suggest a 34.5% drop between 2019 and 2020 (Fig. 5, right panel).  
321 This reduction in NO<sub>x</sub> emissions is significantly larger than the long-term decline of approx. 4% yr<sup>-1</sup> reported in  
322 previous studies for the eastern U.S. and New York City (Krotkov et al., 2016; Goldberg et al., 2019a), and suggests  
323 that COVID-19 measures during the first pandemic wave led to ~30% reduction in NO<sub>x</sub> emissions in New York City,  
324 on top of the long-term trend resulting from air-quality regulations and technological improvements. The reason NO<sub>2</sub>  
325 changes are smaller than NO<sub>x</sub> changes during the coincident timeframe ( $\Delta\text{NO}_2$ : ~24% vs.  $\Delta\text{NO}_x$ : ~35%) is because  
326 there is a background component to NO<sub>2</sub>.

327

328 The EPA National Emissions Inventory (NEI) provides context for expected changes in NO<sub>x</sub> emissions due to the  
329 COVID-19 pandemic. According to 2017 NEI data, mobile sources account for about 59% of annual NO<sub>x</sub> emissions  
330 in New York City (25% on-road, and 34% non-road transportation including non-road equipment (15%) and  
331 locomotives/aircrafts/marine vessels (19%)). The next largest contributing sector is energy (41%), which includes  
332 electric generation, and residential, commercial, and industrial fuel combustion. Wildfires, biogenic sources, and  
333 waste disposal contribute a negligible amount (<1%; NEI 2017). New York City NO<sub>x</sub> emissions are more heavily  
334 weighted in the energy sector than other major U.S. cities such as Los Angeles (13%) and Chicago (26%) (NEI, 2017).  
335 During spring 2020, MTA bridge and tunnel traffic decreased on average by 55%, nation-wide commercial passenger  
336 airline and business aviation travel decreased by approx. 75% and 70% (Transportation Research Board 2020;  
337 FlightAware 2020; Bureau of Transportation Statistics (BTS) 2020), while operation of commercial marine vessels,

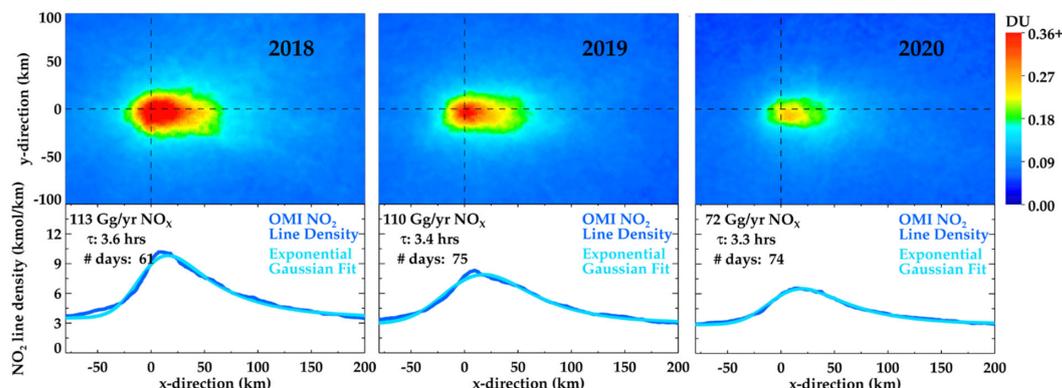


Figure 5: Five-month averaged (May-September) top-down NO<sub>x</sub> emission estimates for the New York metropolitan area, for 2018 (left panel), 2019 (middle panel) and 2020 (right panel). TROPOMI NO<sub>2</sub> data is rotated based on daily wind direction. Bottom panels show the TROPOMI NO<sub>2</sub> line densities, which are integrals along the y-axis  $\pm 50$  km about the x-axis. The statistical EMG fit to the top-down line densities is shown in light blue.



338 non-road equipment, and locomotives dropped by an estimated ~6%, ~45%, and ~15-20%, respectively (United  
339 Nations Conference on Trade and Development 2020; Procore, 2020; BTS 2020). These changes in mobility  
340 correspond approx. to 26% change in NO<sub>x</sub> emissions. Declines in power generation demand/usage in New York City,  
341 however, were considerably smaller, on average 15% in spring 2020 (New York Independent Systems Operator,  
342 2020). These changes in emissions from the transportation and power generation sector suggest approximately 32%  
343 decrease in NO<sub>x</sub> emissions in New York City during the first wave of the pandemic, which is consistent with our  
344 estimated reduction in top-down NO<sub>x</sub> emissions from TROPOMI.

345  
346 The overall less dramatic declines in TCNO<sub>2</sub> observed at locations outside Manhattan (e.g., CT and NJ) during the  
347 first two months following the initial lockdowns agree with reported changes in population, with many city residents  
348 across the US relocating (temporally and long term) to their suburban areas, more so from wealthier than lower-income  
349 neighborhoods (Quealy et al., 2020). They are also consistent with mobility trends across our study region, with the  
350 strongest mobility declines occurring in New York City. According to Apple mobility data, transportation associated  
351 with driving and transit during March-May 2020 were 36% and 72% lower than baseline, respectively, in New York  
352 City, compared to 32% and 54% in Middlesex County NJ and 19% and 49% in New Haven, CT (Fig. S3). Moreover,  
353 the mobile sector constitutes a larger portion of total NO<sub>x</sub> emissions in Middlesex County NJ (72%) and New Haven  
354 CT (71%) than in New York City, with significantly larger contributions from diesel at 36% of Middlesex total  
355 emissions (22% in CT, 25% in NYC). National U.S diesel sales experienced a relatively smaller decrease from 2019  
356 – 2020 than gasoline sales did, with a maximum decrease of ~10% in spring (vs. a mean -40% for gas) (U.S. Energy  
357 Information Administration, 2021), so the relatively larger contribution from diesel in NJ could also partially explain  
358 the smaller decreases in NO<sub>2</sub> at these locations compared to those observed in NY.

### 359 3.3 Changes in NO<sub>2</sub> weekly cycles during the pandemic

360 Anthropogenic NO<sub>x</sub> emissions often display a clear weekly cycle in major cities around the world, with minima on  
361 rest days (e.g., Beirle et al., 2003; Kaynak et al., 2009; Tzortziou et al., 2013). The amplitude of this weekly cycle has  
362 been shown in OMI data (2015-2017) to be strengthening in regions undergoing rapid emission growth, while it has  
363 been weakening over European and U.S. cities due to the long-term decline in anthropogenic emissions (Stavrakou et  
364 al., 2020). Yet, recent data from TROPOMI (2018-2019) show that large NO<sub>2</sub> column decreases on Sunday are still  
365 prevalent in cities of North America, Europe, Australia, Korea and Japan (Stavrakou et al., 2020). In New York City,  
366 TROPOMI captured 30% lower NO<sub>2</sub> on Sundays compared to a typical weekday in 2018-2019 (Goldberg et al., 2021),  
367 in agreement with pre-pandemic MTA and Apple data showing lower traffic into and around the city on Sundays.  
368 Similarly, Pandora measurements in Manhattan showed a clear weekly NO<sub>2</sub> dependence before the pandemic, with  
369 minima consistently observed on Sunday on average 33% lower than weekday values (Figs. 6, 7). A strong diurnal  
370 variability in NO<sub>2</sub> was also found (e.g., Fig 8), although diurnal patterns were highly variable spatially and temporally,  
371 consistent with previous studies (Tzortziou et al., 2013). The Sunday-to-weekday column NO<sub>2</sub> ratio varied seasonally  
372 from 0.64 and 0.63 in spring and summer, to 0.75 and 0.88, respectively, in fall and winter (Figs. 6, 7b), most likely



373 due to the longer tropospheric  $\text{NO}_2$  lifetime and an increase in relative contribution of  $\text{NO}_x$  sources that have no weekly  
 374 cycle (e.g., heating) in winter (Beirle et al., 2003).  
 375  
 376 The COVID-19 measures significantly impacted this weekly  $\text{NO}_2$  behavior. Over the nine months following the  
 377 lockdown in New York (Apr–Nov 2020), TROPOMI captured a clear increase in the Sunday-to-weekday column  $\text{NO}_2$   
 378 ratio from 0.76 to 0.92 (Fig. 7a). Higher frequency Pandora measurements enabled comparison on seasonal timescales,  
 379 revealing a disproportionate drop in weekday  $\text{TCNO}_2$  immediately after the initial lockdown (Figs. 6, 7). Weekday  
 380  $\text{NO}_2$  decreased by as much as 36% and 29% in spring and summer 2020, respectively, while Sunday  $\text{NO}_2$ , decreased

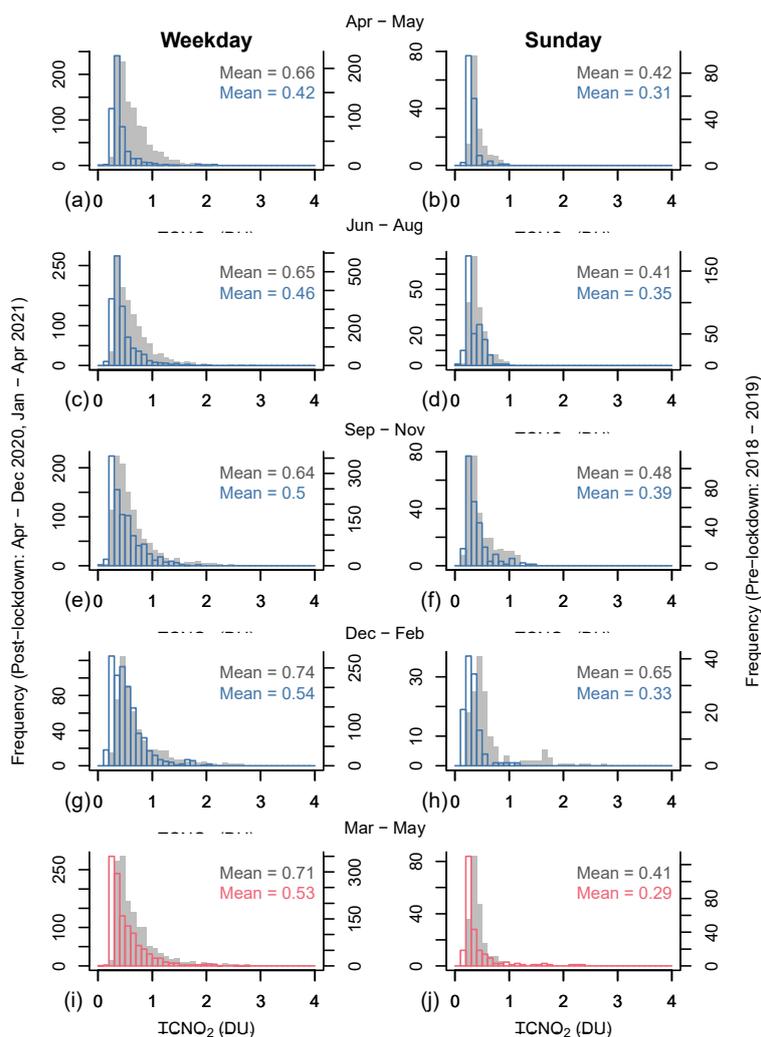


**Figure 6:** Histogram of  $\text{TCNO}_2$  measured in Upper West Manhattan by PSI#135 for pre-lockdown (grey, 2018–2019) and post-lockdown winter (blue) and post-lockdown spring (pink) conditions. Results are shown for weekdays (left column) and Sunday (right column) across seasons from April 2020 to May 2021. The mean  $\text{NO}_2$  pre- and post-lockdown is also shown.



381 only by 26% and 15% (Fig. 6). The Sunday-to-weekday column  $\text{NO}_2$  ratio, thus, increased by 16% in the post-  
382 pandemic spring months with a similar trend into the summer (Fig. 7b). By fall, although  $\text{TCNO}_2$  was still significantly  
383 lower than pre-pandemic levels (-22% on weekdays and -19% on Sundays, Fig. 6), the typical weekly cycle re-  
384 emerged with a post-pandemic ratio of 0.78. Surprisingly, the weekly cycle in  $\text{TCNO}_2$  increased during the winter  
385 (Fig. 7b), as a result of a larger decrease in Sunday  $\text{NO}_2$  (49%) compared to weekday  $\text{NO}_2$  (27%, Fig. 6). A large  
386 departure from typical weekend travel patterns during the second wave of the pandemic, with MTA bridge and tunnel  
387 traffic data showing a relatively larger decrease in traffic on Sundays during winter 2021 (Fig. S3), could partly explain  
388 these results while the adoption of socially distanced protocols by 2021 may have resulted in relatively fewer  
389 reductions of weekday activities such as construction or shipping. By the reopening phase in March-May 2021, the  
390 weekly  $\text{NO}_2$  cycle strengthened significantly (Fig 7b). With the exception of two Sundays in March and April that  
391 showed high peaks in  $\text{TCNO}_2$  due to strong influence of low-speed ( $<5 \text{ ms}^{-1}$ ) south and westerly winds, the Sunday-  
392 to-weekday ratio approached pre-pandemic levels in spring 2021, likely reflecting a return to “normal” as the city-  
393 wide COVID infection rate dropped (Fig. S1).

394

395 Long-term declines in anthropogenic  $\text{NO}_x$  emissions and the resulting growing importance of background  $\text{NO}_2$  had  
396 already led to a significant dampening of the weekly  $\text{NO}_2$  cycle in pre-pandemic New York City over the past 15  
397 years, as shown by an increase in the OMI retrieved Sunday-to-week column ratio by 17% from 2005 to 2017 (Qu et  
398 al., 2021; Stavrakou et al., 2020). Interestingly, the early stringent COVID-19 lockdown measures and related abrupt  
399 changes in human behavior resulted in an additional 16% weakening of the  $\text{NO}_2$  weekly cycle, in just three months.  
400 Including these changes (both weakening and recovery) in weekly cycles of emissions and pollutant concentrations in  
401 chemistry-transport models is important in efforts to quantify and simulate the impacts of the COVID-19 pandemic  
402 on regional air quality, human health, and ecosystems.

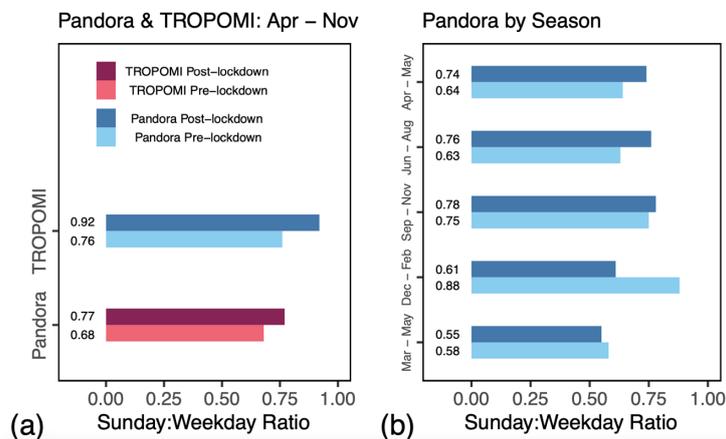


Figure 7: (a) Sunday-to-weekday  $\text{TCNO}_2$  ratios averaged over Apr-Nov 2018–2019 (pre-lockdown) and 2020 (post-lockdown) from TROPOMI and Pandora (PSI#135); (b) Seasonal change in Sunday-to-weekday column ratios pre- and post-lockdown from Pandora (PSI#135).



### 403 3.4. Meteorology as a driver of NO<sub>2</sub> decline and high pollution episodes during the pandemic

404 Despite the significant reduction in NO<sub>2</sub> emissions during and following the COVID-19 lockdown, both ground-based  
405 and satellite sensors captured cases of high pollution in the New York metropolitan region with column NO<sub>2</sub> often  
406 exceeding three times the pre-pandemic levels (Table 1, Figs. 4, 8). April 23 and 25, 2020, during the initial lockdown,  
407 are such instances of TCNO<sub>2</sub> exceeding 1.8 DU (three times the pre-pandemic seasonal NO<sub>2</sub> mean) and showing  
408 remarkably similar diurnal behavior at the Manhattan and Queens locations (Figs. 8c, d). TROPOMI data was not  
409 available, but OMI captured NO<sub>2</sub> > 1 DU over New York city on April 25 (data not shown here). At the early stage  
410 of the second wave of the pandemic, TCNO<sub>2</sub> also exceeded 1.8 DU on October 9 in both Manhattan and Queens with  
411 a time-lag of approximately 2 hours between the maximum observed by the two instruments (Fig. 8e). On the same  
412 day, TROPOMI TCNO<sub>2</sub> reached 0.9 DU, more than two times higher than the pre-pandemic satellite monthly NO<sub>2</sub>  
413 mean (Fig. 8e). Overall, there were 12 days when ground-based measured TCNO<sub>2</sub> exceeded 1.8 DU in post COVID-  
414 19 New York City, despite a 34.5% drop in top-down NO<sub>x</sub> emissions (Fig. 5). Considering the significant decline in  
415 transportation emissions, the post-lockdown high NO<sub>2</sub> pollution episodes are most likely associated with power plant  
416 emissions and specific meteorological conditions. Indeed, the EDGAR v5.0 inventory shows that spatial patterns in  
417 NO<sub>x</sub> emissions over the New York metropolitan area are primarily driven by the power generation sector, while  
418 contributions from road traffic, buildings, and manufacturing show more even distribution with slight peaks of

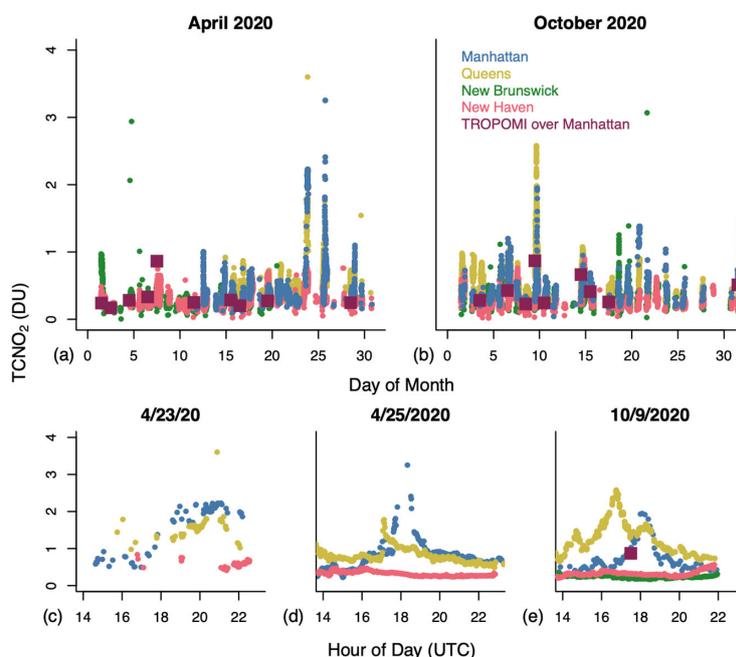
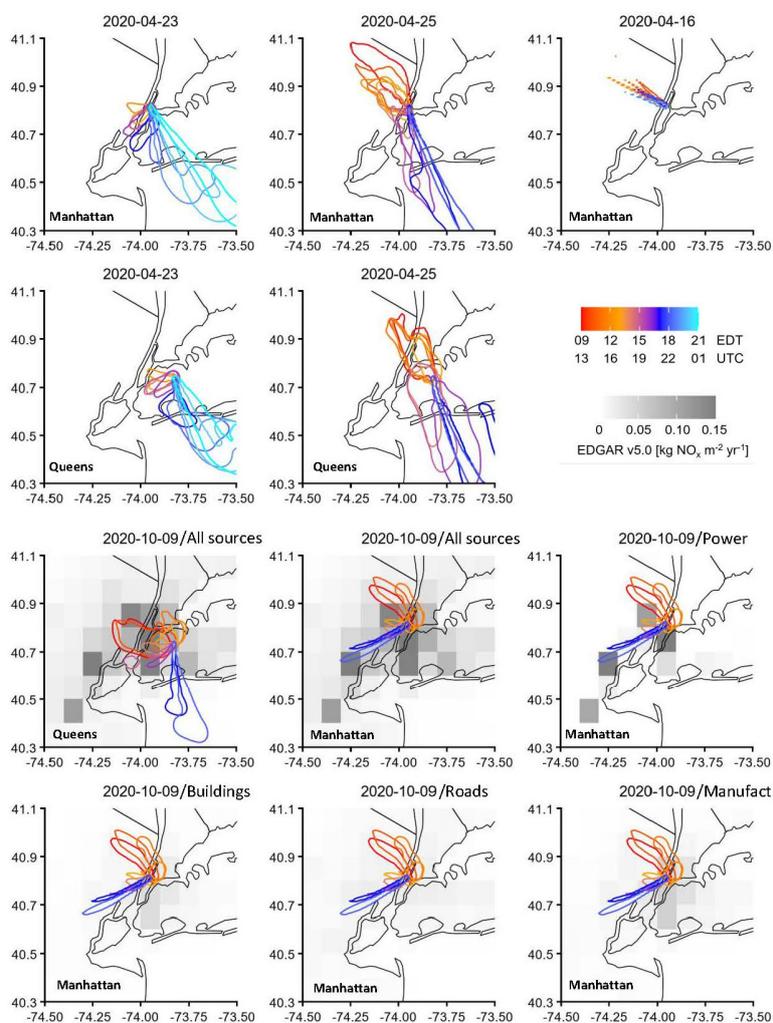


Figure 8: Despite the decline in traffic and physical distancing restrictions, cases of exceedances (TCNO<sub>2</sub> > 1.8 DU) were observed in the New York metropolitan area during and post the COVID-19 lockdown. TCNO<sub>2</sub> measurements are shown here for (a) April 2020 and (b) October 2020, from TROPOMI and Pandora systems in Manhattan, Queens, New Brunswick, and New Haven. Diurnal dynamics in TCNO<sub>2</sub> during specific days of exceedances are shown for (c) April 23, (d) April 25 (no TROPOMI data available), and (e) October 9.



419 approximately  $0.05 \text{ kg NO}_x \text{ m}^{-2}\text{yr}^{-1}$  in Brooklyn, Queens, and Manhattan (Fig. 9). Among the many power plants in  
420 the area, the Astoria Energy LLC and Astoria and Ravenswood Generating Stations in Queens were among the largest  
421 greenhouse gas polluters in the state of NY in 2018 and 2019, with total reported greenhouse emissions  $>3,500,000$   
422 metric tons  $\text{CO}_2\text{e}$  (EPA FLIGHT GHG Inventories) (Fig. 1). In NJ, the PSEG Bergen Generating Station in Ridgefield  
423 (NW of Manhattan/NW of Harlem) and the Linden Cogeneration Facility (SW of Manhattan) are major power plants  
424 located West of Manhattan with total reported emissions  $>7,000,000$  metric tons  $\text{CO}_2\text{e}$  both in 2018 and 2019.



**Figure 9:** Twenty-four hour total STILT surface influence contours for total column  $\text{NO}_2$  exceedances on (a) April 23, (b) April 25, and (c) October 9, 2020, and a low  $\text{NO}_2$  case on (c) April 16, 2020 for comparison. Contour lines represent surface influence of  $1 \text{ ppb}$  ( $\mu\text{mol m}^{-2} \text{ s}^{-1}$ ) and are colored by hour-of-day of the receptor. October 9 is overlaid with EDGAR inventories of  $\text{NO}_x$  for 2015 ( $\text{kg NO}_x \text{ m}^{-2}\text{yr}^{-1}$ ). The area encircled by each contour indicates the region of emissions that reaches the Manhattan and Queens observation sites for a given time and day.



425 Consistent with the location of these power plants, we found that meteorological conditions on days when high  $\text{NO}_2$   
426 was measured in Manhattan were characterized by low-speed southerly and westerly winds. STILT footprints showed  
427 that on April 23 air masses from the high-emitting power sector in NJ and along the East River persisted over Upper  
428 West Manhattan from 1600 to 2100 UTC (Fig. 9) when  $\text{TCNO}_2$  peaked in PSI #135 observations (Fig. 8c). A strong  
429 increase in wind speed and change in direction, effectively mixing in clean ocean air, after 2100 UTC coincided with  
430 a rapid decline in measured  $\text{TCNO}_2$ . A similar pattern was observed on April 25 (Figs. 8d, 9), when air intercepted by  
431 the Manhattan and Queens Pandoras shifts from the NW to SE, slowing while passing over NJ and the East River  
432 power plants around 1800 UTC to produce the observed  $\text{TCNO}_2$  peak at these sites. On October 9, westerly airflow  
433 from NJ shifted to accumulate  $\text{NO}_x$  emissions over the Manhattan Pandora location from 1700 to 1900 UTC when  
434 observed  $\text{TCNO}_2$  peaked at 1.95 DU. Wind accelerated and shifted SW in the evening, coinciding with a  $\text{TCNO}_2$   
435 decrease to  $<0.5$  DU (Figs. 8e, 9). Low-speed westerly winds brought Manhattan and East River power plant emissions  
436 to the Queens location approximately 2 hours earlier that day, in agreement with the earlier peak in  $\text{TCNO}_2$  measured  
437 by the Pandora (Fig. 8e). Strong winds, persisting in a single direction for several hours, consistently dispersed  
438 pollution resulting in low  $\text{NO}_2$  column amounts over Manhattan and Queens. An example is April 16 (Fig. 9), when  
439 high-speed NW winds persisted throughout the day dispersing local and regional pollution and transporting  $\text{NO}_2$  out  
440 to the ocean.

441

442 Combining the STILT footprints, which account for the meteorology described above, with the sector-specific  
443 EDGAR  $\text{NO}_x$  emission maps allows us to approximate the fraction of expected  $\text{NO}_x$  concentration enhancements  
444 from each emission sector observed at each Pandora station. For 25 April, we find that the largest contribution of  $\text{NO}_x$   
445 at the Manhattan site is from power generation (42%), with manufacturing dominating at the Queens site (30%). Road  
446 transportation (using pre-pandemic estimates) contributes only 13% and 18% at the Manhattan and Queens sites,  
447 respectively. Notably, despite the constant emissions rate in EDGAR, the diurnal pattern in near-surface total  $\text{NO}_x$   
448 concentration enhancement matched well with the observed  $\text{TCNO}_2$  observed by the Pandoras on both 23 and 25 April  
449 (not shown here). This result supports the large role played by meteorology in causing  $\text{NO}_2$  accumulation and

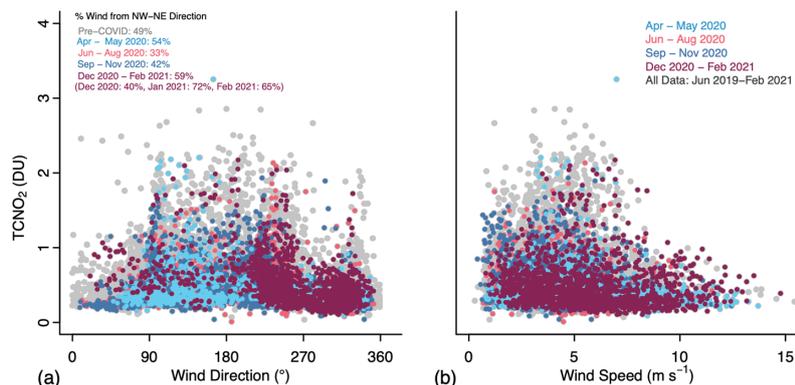


**Figure 10: Relationship between column  $\text{NO}_2$  amounts (DU, PSI #135 data, 15-min averaged) and (a) wind direction (in degrees from north) and (b) wind speed (in  $\text{m s}^{-1}$ ; ATMOS 41 data) organized by post-lockdown season, measured from June 2019 to February 2021 in Upper West Manhattan.**



450 demonstrates a clear connection between the near-surface and total column NO<sub>x</sub> concentrations on these days.  
451  
452 Our measurements showed that the observed correlation between particularly high post-pandemic NO<sub>2</sub> pollution  
453 episodes and low-speed winds is typical of NO<sub>2</sub> dynamics in Manhattan. In large cities with relatively flat topography,  
454 including New York City, increasing wind speeds from nearly stagnant to >8 m s<sup>-1</sup> were previously shown to decrease  
455 NO<sub>2</sub> by 40–85% (Goldberg et al., 2020). Indeed, coincident measurements of wind conditions and NO<sub>2</sub> at the  
456 Manhattan Pandora location before the pandemic showed that TCNO<sub>2</sub> rarely rose above 1 DU at wind speeds faster  
457 than 8 m s<sup>-1</sup> (Fig. 10b). The highest TCNO<sub>2</sub> amounts occurred when surface winds were in the range 1-5 m s<sup>-1</sup>. Under  
458 such conditions, winds are strong enough to transport pollution from local sources as well as major pollutant emitters  
459 in the tri-state area but can still lead to accumulation of pollution in Manhattan.  
460 Moreover, the frequency of high NO<sub>2</sub> pollution events varies by wind direction, which correlate with sources of NO<sub>x</sub>  
461 pollution. Most events with TCNO<sub>2</sub> > 1 DU, and all cases with TCNO<sub>2</sub> > 2DU, occurred with SE-SW winds (90-270°  
462 in Fig. 10a). These air mass origins encompass influences from Queens and Brooklyn (SE), lower Manhattan, and  
463 northern New Jersey (SW-W) where most of the major power plants and economic activity are located (Fig. 1). Mean  
464 TCNO<sub>2</sub> for SE-SW winds was 0.6 DU, compared to 0.4 DU for NE-NW winds. Pre-pandemic TROPOMI retrievals  
465 (2018-2019) also showed that SE-SW winds yield the highest NO<sub>2</sub> levels in New York City, on average twice as high  
466 compared to winds from the NW and NE (Fig. 11), where there are fewer upwind sources. Satellite imagery over the  
467 2018-2019 period was evenly distributed across SE-SW (high NO<sub>2</sub>) and NW-NE (low NO<sub>2</sub>) wind directions.  
468 TROPOMI retrievals also demonstrate a strong negative relationship between satellite NO<sub>2</sub> columns and wind speed  
469 (Fig. 12), with the highest NO<sub>2</sub> occurring at wind speed < 4 m s<sup>-1</sup> and the lowest at wind speed >6 m s<sup>-1</sup> over the New  
470 York metropolitan area before the pandemic.

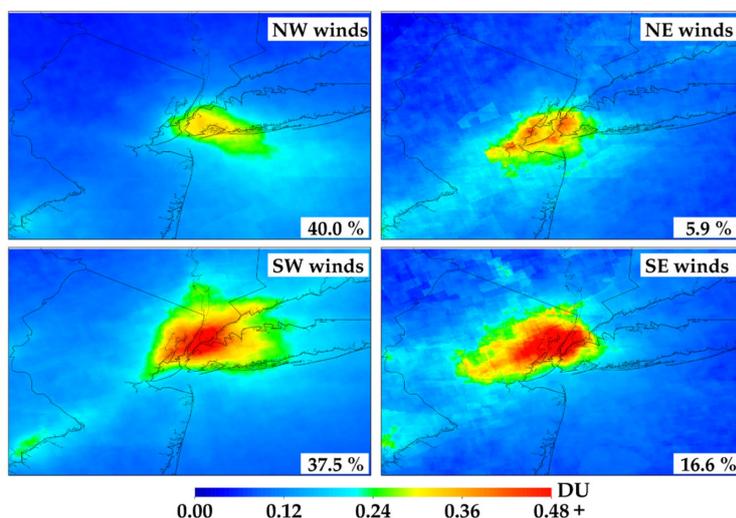


Figure 11: Interpolated TROPOMI NO<sub>2</sub> plumes over New York City in 2018-2019 segregated into 100-m wind direction quadrants NW (top left), NE (top right), SW (bottom left), and SE (bottom right). The percentages of each direction are shown at the bottom right corner of each panel.

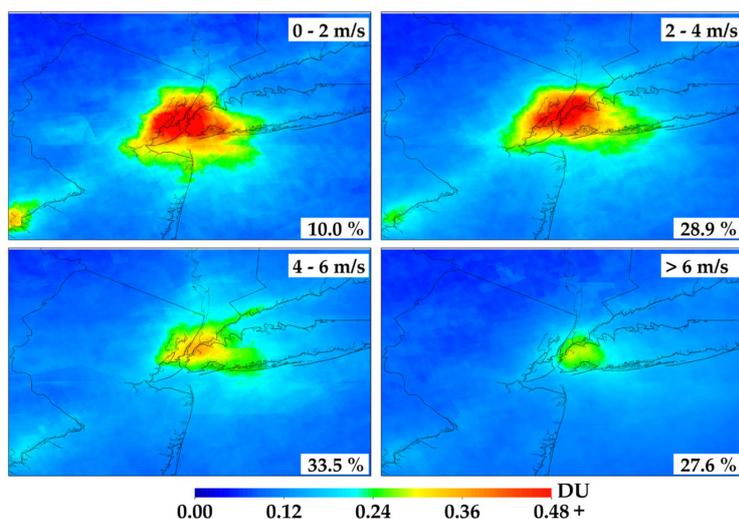


Figure 12: TROPOMI NO<sub>2</sub> segregated by 100-m wind speed in 2 m s<sup>-1</sup> intervals from ERA5 daily meteorology. The percentages of each wind-speed interval are shown at the bottom right corner of each panel.

471

472 These meteorological factors, in addition to explaining the particularly high TCNO<sub>2</sub> values measured even under strict  
473 social distancing restrictions during the COVID-19 lockdowns in the tri-state area, were also found to contribute to  
474 the significantly reduced NO<sub>2</sub> values in winter 2021. January and February 2021 showed a drop in NO<sub>2</sub> by 39% and  
475 30%, respectively, similar to the NO<sub>2</sub> decline observed immediately after the initial strict lockdowns (Fig. 4). Although  
476 traffic (based on both MTA data and Apple mobility trends) showed a noticeable decrease during the second wave of  
477 the pandemic, mobility was not nearly as restricted as in April-May 2020 (Figs. S1-S3). Bridge and tunnel traffic was  
478 approximately 30% lower in winter 2021 compared to 55% lower in spring 2020. Interestingly, in winter 2021 wind  
479 in Upper West Manhattan was mostly (72% in January and 65% in February) from NW-NE directions, which yields  
480 the cleanest conditions and favors low NO<sub>2</sub> columns (Fig. 10a). For comparison, wind at the same location in January  
481 and February 2020 was 49% and 50% from NW-NE direction. In contrast to winter 2021, in spring, summer, and fall  
482 2020, wind was 54%, 33% and 42% from NW-NE directions (compared to 49% in pre-covid conditions, Fig. 10) and  
483 mean wind speed was in the range 3.8-5.5 m s<sup>-1</sup>, suggesting that wind conditions were not favorable for lower NO<sub>2</sub> in  
484 Manhattan in 2020. Hence, our estimates of NO<sub>2</sub> decline in April-December 2020 primarily reflect the impact of  
485 changes in anthropogenic emissions, particularly reductions in emissions from the transportation sector. These  
486 findings corroborate results from Goldberg et al., (2020), who concluded that varying meteorological conditions (wind  
487 speed and direction) in New York City, while different between years, did not have a strong biasing effect in their  
488 estimates of the effects of COVID-19 physical distancing on NO<sub>2</sub> in the month directly following the initial  
489 lockdowns. The prevalence of northerly winds in winter 2021, however, minimized the relative contribution of  
490 emissions from the energy sector to New York City, favoring low NO<sub>2</sub> conditions. This led to stronger NO<sub>2</sub> declines  
491 compared to pre-pandemic levels than would be expected based on just changes in emissions from the transportation  
492 sector during the second wave of the pandemic.



#### 493 4. Summary and conclusions

494 Stringent lockdown measures following the COVID-19 outbreak resulted in an abrupt and significant decline in  
495 TROPOMI top-down NO<sub>x</sub> emissions in New York City, by ~30% on top of long-term trends. A sudden drop in total  
496 column NO<sub>2</sub> (by up to 36% in Manhattan), along with a weakening of the weekly NO<sub>2</sub> cycle and a disruption of typical  
497 seasonal patterns were observed by the ground-based Pandora network in the New York metropolitan area. Yet, during  
498 the same timeframe, traffic in New York City bridges and tunnels plummeted by 55%, on average, compared to pre-  
499 pandemic levels, reaching as much as 80% reduction in early April 2020. These results highlight that although on-  
500 road transportation is an important source of emissions in New York City, emissions from non-road transportation  
501 and the power generation sector (not as strongly affected by the lockdown measures) critically affect NO<sub>2</sub> pollution  
502 levels in New York. Accounting for each sector's contribution to total emissions, resulted in a change in NO<sub>x</sub>  
503 emissions by approx. 32%, which was consistent with satellite top-down estimates.

504

505 Disentangling the impacts of meteorology and NO<sub>x</sub> emission changes on urban air quality is key for designing and  
506 implementing improved emission-control strategies. Meteorology had different impacts across the different pandemic  
507 waves in New York City. Although it was not found to have a strong biasing effect after the first pandemic wave in  
508 spring to fall 2020, meteorology strongly favored clean air conditions over Manhattan after the second pandemic wave  
509 in winter 2021, lowering NO<sub>2</sub> levels beyond what would be expected based on lockdown measures alone. The key  
510 role that meteorology plays in shaping the relative contributions from different emission sectors to NO<sub>2</sub> pollution in  
511 New York City was further demonstrated by the occurrence of several high NO<sub>2</sub> pollution events even during – and  
512 despite - the extreme reductions in transportation emissions during the stringent early lockdowns. High NO<sub>2</sub> columns,  
513 often exceeding three times the pre-pandemic levels, were consistently characterized by low-speed (< 5 m s<sup>-1</sup>) SW-SE  
514 winds that enhanced contributions from the high-emitting power-generation sector and accumulation of pollution over  
515 New York City. A subsequent increase in wind speed and change in wind direction typically coincided with a decrease  
516 in NO<sub>2</sub> over the city, indicating dispersion of pollutants across the coastal environment with potentially negative  
517 effects on downwind communities as well as terrestrial and aquatic ecosystems (Loughner et al., 2016).

518

519 The COVID-19 pandemic resulted in immediate and multifaceted impacts on human behavior that affected various  
520 pollutant sectors and their relative contributions to urban NO<sub>x</sub> emissions differently. During this extreme natural  
521 experiment, long-term and high-temporal resolution retrievals from the Pandora network were essential in capturing  
522 the response of column NO<sub>2</sub> – declines and high pollution episodes - during the multiple pandemic waves and  
523 reopening phases in the New York metropolitan area. Incorporating observed NO<sub>x</sub> emissions changes across  
524 timescales is important for improving air quality modeling and forecasting, especially in the context of sub-daily  
525 stagnation events that produce NO<sub>x</sub> exceedances despite low emissions. Such high-resolution observations from  
526 ground-based networks, and soon from geostationary satellite sensors such as TEMPO (Chance et al., 2013), enable  
527 the characterization of fine-scale features in NO<sub>2</sub> behavior as well as assessment of the possible effects of rapid  
528 meteorological changes on air quality conditions. In New York, a city transitioning to a NO<sub>x</sub> limited ozone production  
529 environment during summer (Jin et al., 2017), NO<sub>x</sub> plays an important role in the oxidation of VOC's ozone



530 production as well as secondary aerosol formation. Integration of high-resolution NO<sub>2</sub> measurements from ground-  
531 based networks and geostationary satellite platforms is, thus, critical in further assessing changes in NO<sub>2</sub>, aerosol, and  
532 ozone pollution as the world re-opens, and in evaluating the effectiveness of future sector-specific NO<sub>x</sub> emission  
533 control strategies and their impacts on air quality, human health, and urban ecosystems.

534 **Acknowledgements:** We thank Alexander Cede, Thomas Hanisco, Moritz Mueller, Michael Gray, Elena Spinei Lind,  
535 Brian Lamb and the NASA Pandora Project and ESA Pandonia Project staff for assistance in the field and for  
536 establishing and maintaining the Pandora sites used in this investigation. We also thank Rohit Mathur and Venkatesh  
537 Rao for feedback on an earlier draft of this manuscript. This research was supported by NASA Rapid Response and  
538 Novel research in the Earth Sciences (RRNES) Program, grant number 80NSSC20K1287, NASA Interdisciplinary  
539 Science (IDS) Program, grant 80NSSC17K0258, NOAA Earth System Sciences and Remote Sensing Technologies  
540 award NA16SEC4810008, and NOAA Climate Program Office's Atmospheric Chemistry, Carbon Cycle, and Climate  
541 program, grant number NA20OAR4310306.

542 **Disclaimer:** The research described in this article has been reviewed by the U.S. Environmental Protection Agency  
543 (EPA) and approved for publication. Approval does not signify that the contents necessarily reflect the views and the  
544 policies of the agency nor does mention of trade names or commercial products constitute endorsement or  
545 recommendation for use.



## 546 References

- 547 A, R. J. van der, Eskes, H. J., Boersma, K. F., Noije, T. P. C. van, Roozendael, M. V., Smedt, I. D., Peters, D. H. M.  
548 U., and Meijer, E. W.: Trends, seasonal variability and dominant NO<sub>x</sub> source derived from a ten year record  
549 of NO<sub>2</sub> measured from space, *J. Geophys. Res. Atmos.*, 113, <https://doi.org/10.1029/2007JD009021>, 2008.
- 550 Apple COVID-19 Mobility Trends Reports: <https://www.apple.com/covid19/mobility>, last access: 4 June 2021.
- 551 Banta, R. M., Senff, C. J., Alvarez, R. J., Langford, A. O., Parrish, D. D., Trainer, M. K., Darby, L. S., Michael  
552 Hardesty, R., Lambeth, B., Andrew Neuman, J., Angevine, W. M., Nielsen-Gammon, J., Sandberg, S. P.,  
553 and White, A. B.: Dependence of daily peak O<sub>3</sub> concentrations near Houston, Texas on environmental  
554 factors: Wind speed, temperature, and boundary-layer depth, *Atmospheric Environment*, 45, 162–173,  
555 <https://doi.org/10.1016/j.atmosenv.2010.09.030>, 2011.
- 556 Barbieri, D. M., Lou, B., Passavanti, M., Hui, C., Hoff, I., Lessa, D. A., Sikka, G., Chang, K., Gupta, A., Fang, K.,  
557 Banerjee, A., Maharaj, B., Lam, L., Ghasemi, N., Naik, B., Wang, F., Mirhosseini, A. F., Naseri, S., Liu, Z.,  
558 Qiao, Y., Tucker, A., Wijayarathna, K., Peprah, P., Adomako, S., Yu, L., Goswami, S., Chen, H., Shu, B.,  
559 Hessami, A., Abbas, M., Agarwal, N., and Rashidi, T. H.: Impact of COVID-19 pandemic on mobility in ten  
560 countries and associated perceived risk for all transport modes, *PLOS ONE*, 16, e0245886,  
561 <https://doi.org/10.1371/journal.pone.0245886>, 2021.
- 562 Bauwens, M., Compennolle, S., Stavrakou, T., Müller, J.-F., Gent, J. van, Eskes, H., Levelt, P. F., A, R. van der,  
563 Veefkind, J. P., Vlietinck, J., Yu, H., and Zehner, C.: Impact of Coronavirus Outbreak on NO<sub>2</sub> Pollution  
564 Assessed Using TROPOMI and OMI Observations, *Geophys. Res. Lett.*, 47, e2020GL087978,  
565 <https://doi.org/10.1029/2020GL087978>, 2020.
- 566 Beirle, S., Platt, U., Wenig, M., and Wagner, T.: Weekly cycle of NO<sub>2</sub> by GOME measurements: a signature of  
567 anthropogenic sources, *Atmos. Chem. Phys.*, 3, 2225–2232, <https://doi.org/10.5194/acp-3-2225-2003>, 2003.
- 568 Beirle, S., Boersma, K. F., Platt, U., Lawrence, M. G., and Wagner, T.: Megacity Emissions and Lifetimes of Nitrogen  
569 Oxides Probed from Space, *Science*, 333, 1737–1739, <https://doi.org/10.1126/science.1207824>, 2011.
- 570 Beirle, S., Borger, C., Dörner, S., Li, A., Hu, Z., Liu, F., Wang, Y., and Wagner, T.: Pinpointing nitrogen oxide  
571 emissions from space, *Sci. Adv.*, 5, eaax9800, <https://doi.org/10.1126/sciadv.aax9800>, 2019.
- 572 Berman, J. D. and Ebisu, K.: Changes in U.S. air pollution during the COVID-19 pandemic, *Science of The Total*  
573 *Environment*, 739, 139864, <https://doi.org/10.1016/j.scitotenv.2020.139864>, 2020.
- 574 Boersma, K. F., Eskes, H. J., Richter, A., De Smedt, I., Lorente, A., Beirle, S., van Geffen, J. H. G. M., Zara, M.,  
575 Peters, E., Van Roozendael, M., Wagner, T., Maasackers, J. D., van der A, R. J., Nightingale, J., De Rudder,  
576 A., Irie, H., Pinardi, G., Lambert, J.-C., and Compennolle, S. C.: Improving algorithms and uncertainty  
577 estimates for satellite NO<sub>2</sub> retrievals: results from the quality assurance for the essential climate variables  
578 (QA4ECV) project, *Atmos. Meas. Tech.*, 11, 6651–6678, <https://doi.org/10.5194/amt-11-6651-2018>, 2018.
- 579 Bounds, A. M.: New Yorkers' Street Smarts and Survival Smarts During the Pandemic: Preppers, Community  
580 Resilience and Local Citizenship, *Urbana*, XXI, <https://doi.org/10.47785/urbana.5.2020>, n.d.
- 581 Bureau of Transportation Statistics | The Week in Transportation: [https://www.bts.gov/covid-19/week-in-](https://www.bts.gov/covid-19/week-in-transportation)  
582 [transportation](https://www.bts.gov/covid-19/week-in-transportation), last access: 9 June 2021.



- 583 Burnett, R., Chen, H., Szyszkowicz, M., Fann, N., Hubbell, B., Pope, C. A., Apte, J. S., Brauer, M., Cohen, A.,  
584 Weichenthal, S., Coggins, J., Di, Q., Brunekreef, B., Frostad, J., Lim, S. S., Kan, H., Walker, K. D., Thurston,  
585 G. D., Hayes, R. B., Lim, C. C., Turner, M. C., Jerrett, M., Krewski, D., Gapstur, S. M., Diver, W. R., Ostro,  
586 B., Goldberg, D., Crouse, D. L., Martin, R. V., Peters, P., Pinault, L., Tjepkema, M., Donkelaar, A. van,  
587 Villeneuve, P. J., Miller, A. B., Yin, P., Zhou, M., Wang, L., Janssen, N. A. H., Marra, M., Atkinson, R. W.,  
588 Tsang, H., Thach, T. Q., Cannon, J. B., Allen, R. T., Hart, J. E., Laden, F., Cesaroni, G., Forastiere, F.,  
589 Weinmayr, G., Jaensch, A., Nagel, G., Concin, H., and Spadaro, J. V.: Global estimates of mortality  
590 associated with long-term exposure to outdoor fine particulate matter, *PNAS*, 115, 9592–9597,  
591 <https://doi.org/10.1073/pnas.1803222115>, 2018.
- 592 Burnett, R. T., Stieb, D., Brook, J. R., Cakmak, S., Dales, R., Raizenne, M., Vincent, R., and Dann, T.: Associations  
593 between Short-Term Changes in Nitrogen Dioxide and Mortality in Canadian Cities, *Arch. Environ. Health*,  
594 59, 228–236, <https://doi.org/10.3200/AEOH.59.5.228-236>, 2004.
- 595 Chance, K., Liu, X., Suleiman, R. M., Flittner, D. E., Al-Saadi, J., and Janz, S. J.: Tropospheric emissions: monitoring  
596 of pollution (TEMPO), in: *Earth Observing Systems XVIII*, Earth Observing Systems XVIII, 88660D,  
597 <https://doi.org/10.1117/12.2024479>, 2013.
- 598 COVID-19: Latest Data - NYC Health: <https://www1.nyc.gov/site/doh/covid/covid-19-data.page>, last access: 9 July  
599 2021.
- 600 Decina, S. M., Templer, P. H., Hutyra, L. R., Gately, C. K., and Rao, P.: Variability, drivers, and effects of atmospheric  
601 nitrogen inputs across an urban area: Emerging patterns among human activities, the atmosphere, and soils,  
602 *Science of The Total Environment*, 609, 1524–1534, <https://doi.org/10.1016/j.scitotenv.2017.07.166>, 2017.
- 603 Decina, S. M., Hutyra, L. R., and Templer, P. H.: Hotspots of nitrogen deposition in the world’s urban areas: a global  
604 data synthesis, *J. Ecol. Environ.*, 18, 92–100, <https://doi.org/10.1002/fec.2143>, 2020.
- 605 Dix, B., Bruin, J. de, Roosenbrand, E., Vlemmix, T., Francoeur, C., Gorchov-Negron, A., McDonald, B., Zhizhin, M.,  
606 Elvidge, C., Veeffkind, P., Levelt, P., and Gouw, J. de: Nitrogen Oxide Emissions from U.S. Oil and Gas  
607 Production: Recent Trends and Source Attribution, *Geophys. Res. Lett.*, 47, e2019GL085866,  
608 <https://doi.org/10.1029/2019GL085866>, 2020.
- 609 Duan, Y., Liao, Y., Li, H., Yan, S., Zhao, Z., Yu, S., Fu, Y., Wang, Z., Yin, P., Cheng, J., and Jiang, H.: Effect of  
610 changes in season and temperature on cardiovascular mortality associated with nitrogen dioxide air pollution  
611 in Shenzhen, China, *Science of The Total Environment*, 697, 134051,  
612 <https://doi.org/10.1016/j.scitotenv.2019.134051>, 2019.
- 613 Duncan, B. N., Lamsal, L. N., Thompson, A. M., Yoshida, Y., Lu, Z., Streets, D. G., Hurwitz, M. M., and Pickering,  
614 K. E.: A space-based, high-resolution view of notable changes in urban NO<sub>x</sub> pollution around the world  
615 (2005–2014), *J. Geophys. Res. Atmos.*, 121, 976–996, <https://doi.org/10.1002/2015JD024121>, 2016.
- 616 EPA: Modeling the Interactive Effects from Nitrogen Deposition and Climate Change on Terrestrial Ecosystems and  
617 Biodiversity: [https://www.epa.gov/climate-research/modeling-interactive-effects-nitrogen-deposition-and-](https://www.epa.gov/climate-research/modeling-interactive-effects-nitrogen-deposition-and-climate-change-terrestrial)  
618 [climate-change-terrestrial](https://www.epa.gov/climate-research/modeling-interactive-effects-nitrogen-deposition-and-climate-change-terrestrial), last access: 6 May 2021.
- 619 Fares, S., Vargas, R., Detto, M., Goldstein, A. H., Karlik, J., Paoletti, E., and Vitale, M.: Tropospheric ozone reduces



- 620 carbon assimilation in trees: estimates from analysis of continuous flux measurements, *Global Change Biol.*,  
621 19, 2427–2443, <https://doi.org/10.1111/gcb.12222>, 2013.
- 622 FlightAware - An Uneven Recovery: A Sector-by-Sector Visualization of the Impact of COVID-19 on Aviation:  
623 <https://blog.flightaware.com/visualizing-the-impact-of-covid-19-on-the-aviation-industry>, last access: 9 July  
624 2021.
- 625 Forster, P. M., Forster, H. I., Evans, M. J., Gidden, M. J., Jones, C. D., Keller, C. A., Lamboll, R. D., Quéré, C. L.,  
626 Rogelj, J., Rosen, D., Schleussner, C.-F., Richardson, T. B., Smith, C. J., and Turnock, S. T.: Current and  
627 future global climate impacts resulting from COVID-19, *Nat. Clim. Change*, 10, 913–919,  
628 <https://doi.org/10.1038/s41558-020-0883-0>, 2020.
- 629 de Foy, B., Wilkins, J. L., Lu, Z., Streets, D. G., and Duncan, B. N.: Model evaluation of methods for estimating  
630 surface emissions and chemical lifetimes from satellite data, *Atmospheric Environment*, 98, 66–77,  
631 <https://doi.org/10.1016/j.atmosenv.2014.08.051>, 2014.
- 632 Gately, C. K., Hutyla, L. R., and Wing, I. S.: Cities, traffic, and CO<sub>2</sub>: A multidecadal assessment of trends, drivers,  
633 and scaling relationships, *PNAS*, 112, 4999–5004, <https://doi.org/10.1073/pnas.1421723112>, 2015.
- 634 Gkatzelis, G. I., Gilman, J. B., Brown, S. S., Eskes, H., Gomes, A. R., Lange, A. C., McDonald, B. C., Peischl, J.,  
635 Petzold, A., Thompson, C. R., and Kiendler-Scharr, A.: The global impacts of COVID-19 lockdowns on  
636 urban air pollution: A critical review and recommendations, *Elementa: Science of the Anthropocene*, 9,  
637 <https://doi.org/10.1525/elementa.2021.00176>, 2021.
- 638 Goldberg, D. L., Anenberg, S. C., Griffin, D., McLinden, C. A., Lu, Z., and Streets, D. G.: Disentangling the Impact  
639 of the COVID-19 Lockdowns on Urban NO<sub>2</sub> From Natural Variability, *Geophys. Res. Lett.*, 47,  
640 e2020GL089269, <https://doi.org/10.1029/2020GL089269>, 2020.
- 641 Goldberg, D. L., Anenberg, S. C., Kerr, G. H., Moheg, A., Lu, Z., & Streets, D. G.: TROPOMI NO<sub>2</sub> in the United  
642 States: A detailed look at the annual averages, weekly cycles, effects of temperature, and correlation with  
643 surface NO<sub>2</sub> concentrations. *Earth's Future*, e2020EF001665, <https://doi.org/10.1029/2020EF001665>, 2021
- 644 Goldberg, D. L., Lu, Z., Oda, T., Lamsal, L. N., Liu, F., Griffin, D., et al.: Exploiting OMI NO<sub>2</sub> satellite observations  
645 to infer fossil-fuel CO<sub>2</sub> emissions from U.S. megacities. *Science of the Total Environment*, 695,  
646 <https://doi.org/10.1016/j.scitotenv.2019.133805>, 2019a.
- 647 Goldberg, D. L., Lu, Z., Streets, D. G., de Foy, B., Griffin, D., McLinden, C. A., Lamsal, L. N., Krotkov, N. A., and  
648 Eskes, H.: Enhanced Capabilities of TROPOMI NO<sub>2</sub>: Estimating NO<sub>x</sub> from North American Cities and  
649 Power Plants, *Environ. Sci. Technol.*, 53, 12594–12601, <https://doi.org/10.1021/acs.est.9b04488>, 2019b.
- 650 Griffin, D., Zhao, X., McLinden, C. A., Boersma, F., Bourassa, A., Dammers, E., Degenstein, D., Eskes, H., Fehr, L.,  
651 Fioletov, V., Hayden, K., Kharol, S. K., Li, S.-M., Makar, P., Martin, R. V., Mihele, C., Mittermeier, R. L.,  
652 Krotkov, N., Sneep, M., Lamsal, L. N., Linden, M. ter, Geffen, J. van, Veeffkind, P., and Wolde, M.: High-  
653 Resolution Mapping of Nitrogen Dioxide With TROPOMI: First Results and Validation Over the Canadian  
654 Oil Sands, *Geophys. Res. Lett.*, 46, 1049–1060, <https://doi.org/10.1029/2018GL081095>, 2019.
- 655 Herman, J., Spinei, E., Fried, A., Kim, J., Kim, J., Kim, W., Cede, A., Abuhassan, N., and Segal-Rozenhaimer, M.:  
656 NO<sub>2</sub> and HCHO measurements in Korea from 2012 to 2016 from Pandora spectrometer instruments



- 657 compared with OMI retrievals and with aircraft measurements during the KORUS-AQ campaign, *Atmos.*  
658 *Meas. Tech.*, 11, 4583–4603, <https://doi.org/10.5194/amt-11-4583-2018>, 2018.
- 659 Herman, J., Abuhassan, N., Kim, J., Kim, J., Dubey, M., Raponi, M., and Tzortziou, M.: Underestimation of column  
660 NO<sub>2</sub> amounts from the OMI satellite compared to diurnally varying ground-based retrievals from multiple  
661 PANDORA spectrometer instruments, *Atmos. Meas. Tech.*, 12, 5593–5612, [https://doi.org/10.5194/amt-12-](https://doi.org/10.5194/amt-12-5593-2019)  
662 [5593-2019](https://doi.org/10.5194/amt-12-5593-2019), 2019.
- 663 Hersbach, H., Bell, B., Berrisford, P., Hirahara, S., Horányi, A., Muñoz-Sabater, J., Nicolas, J., Peubey, C., Radu, R.,  
664 Schepers, D., Simmons, A., Soci, C., Abdalla, S., Abellan, X., Balsamo, G., Bechtold, P., Biavati, G., Bidlot,  
665 J., Bonavita, M., Chiara, G. D., Dahlgren, P., Dee, D., Diamantakis, M., Dragani, R., Flemming, J., Forbes,  
666 R., Fuentes, M., Geer, A., Haimberger, L., Healy, S., Hogan, R. J., Hólm, E., Janisková, M., Keeley, S.,  
667 Laloyaux, P., Lopez, P., Lupu, C., Radnoti, G., Rosnay, P. de, Rozum, I., Vamborg, F., Villaume, S., and  
668 Thépaut, J.-N.: The ERA5 global reanalysis, *Q. J. Roy. Meteor. Soc.*, 146, 1999–2049,  
669 <https://doi.org/10.1002/qj.3803>, 2020.
- 670 Ialongo, I., Virta, H., Eskes, H., Hovila, J., and Douros, J.: Comparison of TROPOMI/Sentinel-5 Precursor NO<sub>2</sub>  
671 observations with ground-based measurements in Helsinki, *Atmos. Meas. Tech.*, 13, 205–218,  
672 <https://doi.org/10.5194/amt-13-205-2020>, 2020.
- 673 Judd, L. M., Al-Saadi, J. A., Szykman, J. J., Valin, L. C., Janz, S. J., Kowalewski, M. G., Eskes, H. J., Veeffkind, J. P.,  
674 Cede, A., Mueller, M., Gebetsberger, M., Swap, R., Pierce, R. B., Nowlan, C. R., Abad, G. G., Nehrir, A.,  
675 and Williams, D.: Evaluating Sentinel-5P TROPOMI tropospheric NO<sub>2</sub> column densities with airborne and  
676 Pandora spectrometers near New York City and Long Island Sound, *Atmos. Meas. Tech.*, 13, 6113–6140,  
677 <https://doi.org/10.5194/amt-13-6113-2020>, 2020.
- 678 Karambelas, A.: LISTOS: Toward a Better Understanding of New York City’s Ozone Pollution Problem, *The*  
679 *Magazine for Environmental Managers*, 2020.
- 680 Kaynak, B., Hu, Y., Martin, R. V., Sioris, C. E., and Russell, A. G.: Comparison of weekly cycle of NO<sub>2</sub> satellite  
681 retrievals and NO<sub>x</sub> emission inventories for the continental United States, *J. Geophys. Res. Atmos.*, 114,  
682 <https://doi.org/10.1029/2008JD010714>, 2009.
- 683 Krotkov, N. A., McLinden, C. A., Li, C., Lamsal, L. N., Celarier, E. A., Marchenko, S. V., Swartz, W. H., Bucsela,  
684 E. J., Joiner, J., Duncan, B. N., Boersma, K. F., Veeffkind, J. P., Levelt, P. F., Fioletov, V. E., Dickerson, R.  
685 R., He, H., Lu, Z., and Streets, D. G.: Aura OMI observations of regional SO<sub>2</sub> and NO<sub>2</sub> pollution changes  
686 from 2005 to 2015, *Atmos. Chem. Phys.*, 16, 4605–4629, <https://doi.org/10.5194/acp-16-4605-2016>, 2016.
- 687 Lim, S. S., Vos, T., Flaxman, A. D., Danaei, G., Shibuya, K., Adair-Rohani, H., AlMazroa, M. A., Amann, M.,  
688 Anderson, H. R., Andrews, K. G., Aryee, M., Atkinson, C., Bacchus, L. J., Bahalim, A. N., Balakrishnan,  
689 K., Balmes, J., Barker-Collo, S., Baxter, A., Bell, M. L., Blore, J. D., Blyth, F., Bonner, C., Borges, G.,  
690 Bourne, R., Boussinesq, M., Brauer, M., Brooks, P., Bruce, N. G., Brunekreef, B., Bryan-Hancock, C.,  
691 Bucello, C., Buchbinder, R., Bull, F., Burnett, R. T., Byers, T. E., Calabria, B., Carapetis, J., Carnahan, E.,  
692 Chafe, Z., Charlson, F., Chen, H., Chen, J. S., Cheng, A. T.-A., Child, J. C., Cohen, A., Colson, K. E., Cowie,  
693 B. C., Darby, S., Darling, S., Davis, A., Degenhardt, L., Dentener, F., Des Jarlais, D. C., Devries, K., Dherani,



- 694 M., Ding, E. L., Dorsey, E. R., Driscoll, T., Edmond, K., Ali, S. E., Engell, R. E., Erwin, P. J., Fahimi, S.,  
695 Falder, G., Farzadfar, F., Ferrari, A., Finucane, M. M., Flaxman, S., Fowkes, F. G. R., Freedman, G.,  
696 Freeman, M. K., Gakidou, E., Ghosh, S., Giovannucci, E., Gmel, G., Graham, K., Grainger, R., Grant, B.,  
697 Gunnell, D., Gutierrez, H. R., Hall, W., Hoek, H. W., Hogan, A., Hosgood, H. D., Hoy, D., Hu, H., Hubbell,  
698 B. J., Hutchings, S. J., Ibeanusi, S. E., Jacklyn, G. L., Jasrasaria, R., Jonas, J. B., Kan, H., Kanis, J. A.,  
699 Kassebaum, N., Kawakami, N., Khang, Y.-H., Khatibzadeh, S., Khoo, J.-P., et al.: A comparative risk  
700 assessment of burden of disease and injury attributable to 67 risk factors and risk factor clusters in 21 regions,  
701 1990–2010: a systematic analysis for the Global Burden of Disease Study 2010, *The Lancet*, 380, 2224–  
702 2260, [https://doi.org/10.1016/S0140-6736\(12\)61766-8](https://doi.org/10.1016/S0140-6736(12)61766-8), 2012.
- 703 Liu, F., Page, A., Strode, S. A., Yoshida, Y., Choi, S., Zheng, B., Lamsal, L. N., Li, C., Krotkov, N. A., Eskes, H., A,  
704 R. van der, Veeffkind, P., Levelt, P. F., Hauser, O. P., and Joiner, J.: Abrupt decline in tropospheric nitrogen  
705 dioxide over China after the outbreak of COVID-19, *Sci. Adv.*, 6, eabc2992,  
706 <https://doi.org/10.1126/sciadv.abc2992>, 2020.
- 707 Loughner, C. P., Tzortziou, M., Shroder, S., and Pickering, K. E.: Enhanced dry deposition of nitrogen pollution near  
708 coastlines: A case study covering the Chesapeake Bay estuary and Atlantic Ocean coastline, *J. Geophys. Res.*  
709 *Atmos.*, 121, 14,221–14,238, <https://doi.org/10.1002/2016JD025571>, 2016.
- 710 NY MTA Day-by-day ridership numbers: <https://new.mta.info/coronavirus/ridership>, last access: 4 June 2021.
- 711 Paerl, H. W., Dennis, R. L., and Whittall, D. R.: Atmospheric deposition of nitrogen: Implications for nutrient over-  
712 enrichment of coastal waters, *Estuaries*, 25, 677–693, <https://doi.org/10.1007/BF02804899>, 2002.
- 713 Pardo, L. H., Robin-Abbott, M. J., and C. T., eds D.: Assessment of Nitrogen deposition effects and empirical critical  
714 loads of Nitrogen for ecoregions of the United States, Gen. Tech. Rep. NRS-80, U.S Department of  
715 Agriculture, Forest Service, 80, 1–291, <https://doi.org/10.2737/NRS-GTR-80>, 2011.
- 716 Procure (2020) COVID-19 and Construction Activity [https://www.agc.org/sites/default/files/ Procure Construction](https://www.agc.org/sites/default/files/Procure_Construction)  
717 *Activity Index - Metro Report June 2020\_0.pdf*, last access: 9 July 2021.
- 718 Przybylowski, A., Stelmak, S., and Suchanek, M.: Mobility Behaviour in View of the Impact of the COVID-19  
719 Pandemic—Public Transport Users in Gdansk Case Study, *Sustainability*, 13, 364,  
720 <https://doi.org/10.3390/su13010364>, 2021.
- 721 Qu, Z., Jacob, D. J., Silvern, R. F., Shah, V., Campbell, P. C., Valin, L. C., and Murray, L. T.: US COVID-19  
722 Shutdown Demonstrates Importance of Background NO<sub>2</sub> in Inferring NO<sub>x</sub> Emissions From Satellite NO<sub>2</sub>  
723 Observations, *Geophys. Res. Lett.*, 48, e2021GL092783, <https://doi.org/10.1029/2021GL092783>, 2021.
- 724 Quealy, K.: The Richest Neighborhoods Emptied Out Most as Coronavirus Hit New York City, *The New York Times*,  
725 15th May, 2020.
- 726 Reuter, M., Buchwitz, M., Schneising, O., Krautwurst, S., O’Dell, C. W., Richter, A., Bovensmann, H., and Burrows,  
727 J. P.: Towards monitoring localized CO<sub>2</sub> emissions from space: co-located regional CO<sub>2</sub> and NO<sub>2</sub>  
728 enhancements observed by the OCO-2 and S5P satellites, *Atmos. Chem. Phys.*, 19, 9371–9383,  
729 <https://doi.org/10.5194/acp-19-9371-2019>, 2019.
- 730 Roberts–Semple, D., Song, F., and Gao, Y.: Seasonal characteristics of ambient nitrogen oxides and ground–level



- 731 ozone in metropolitan northeastern New Jersey, *Atmospheric Pollution Research*, 3, 247–257,  
732 <https://doi.org/10.5094/APR.2012.027>, 2012.
- 733 Spinei, E., Whitehill, A., Fried, A., Tiefengraber, M., Knepp, T. N., Herndon, S., Herman, J. R., Müller, M.,  
734 Abuhassan, N., Cede, A., Richter, D., Walega, J., Crawford, J., Szykman, J., Valin, L., Williams, D. J., Long,  
735 R., Swap, R. J., Lee, Y., Nowak, N., and Poche, B.: The first evaluation of formaldehyde column observations  
736 by improved Pandora spectrometers during the KORUS-AQ field study, *Atmos. Meas. Tech.*, 11, 4943–  
737 4961, <https://doi.org/10.5194/amt-11-4943-2018>, 2018.
- 738 Stacey, P. E., Greening, H. S., Kremer, J. N., Peterson, D., and Tomasko, D. A.: Contributions of Atmospheric  
739 Nitrogen Deposition to U.S. Estuaries: Summary and Conclusions, in: *Nitrogen Loading in Coastal Water  
740 Bodies: An Atmospheric Perspective*, American Geophysical Union (AGU), 187–226,  
741 <https://doi.org/10.1029/CE057p0187>, 2001.
- 742 Stavrakou, T., Müller, J.-F., Bauwens, M., Boersma, K. F., and van Geffen, J.: Satellite evidence for changes in the  
743 NO<sub>2</sub> weekly cycle over large cities, *Sci. Rep.*, 10, 10066, <https://doi.org/10.1038/s41598-020-66891-0>,  
744 2020.
- 745 Szykman, J., Swap, R., Lefter, B., Valin, L., Lee, S. C., Fioletov, V., Zhao, X., Davies, J., Williams, D., Abuhassan,  
746 N., Shalaby, L., Cede, A., Tiefengraber, M., Mueller, M., Kotsakis, A., Santos, F., and Robinson, J.: Pandora:  
747 Connecting in-situ and Satellite Monitoring in Support of the Canada - U.S. Air Quality Agreement, EM: Air  
748 and Waste Management Association's Magazine for Environmental Managers, 2019.
- 749 Thakrar, S. K., Balasubramanian, S., Adams, P. J., Azevedo, I. M. L., Muller, N. Z., Pandis, S. N., Polasky, S., Pope,  
750 C. A., Robinson, A. L., Apte, J. S., Tessum, C. W., Marshall, J. D., and Hill, J. D.: Reducing Mortality from  
751 Air Pollution in the United States by Targeting Specific Emission Sources, *Environ. Sci. Technol. Lett.*, 7,  
752 639–645, <https://doi.org/10.1021/acs.estlett.0c00424>, 2020.
- 753 Transportation Research Board Webinar Visualizing Effects of COVID 19 on Transportation A One Year  
754 Retrospective | National Academies: [https://www.nationalacademies.org/event/03-08-2021/trb-webinar-  
755 visualizing-effects-of-covid-19-on-transportation-a-one-year-retrospective](https://www.nationalacademies.org/event/03-08-2021/trb-webinar-visualizing-effects-of-covid-19-on-transportation-a-one-year-retrospective), last access: 9 July 2021.
- 756 Tzortziou M., O. Parker, B. Lamb, J. R. Herman, L. Lamsal, R. Stauffer and N. Abuhassan: Atmospheric Trace Gas  
757 (NO<sub>2</sub> and O<sub>3</sub>) Variability in South Korean Coastal Waters, and Implications for Remote Sensing of Coastal  
758 Ocean Color Dynamics. *Remote Sens.* 10(10), 1587; <https://doi.org/10.3390/rs10101587>, 2018.
- 759 Tzortziou, M., Herman, J. R., Ahmad, Z., Loughner, C. P., Abuhassan, N., and Cede, A.: Atmospheric NO<sub>2</sub> dynamics  
760 and impact on ocean color retrievals in urban nearshore regions, *J. Geophys. Res. Oceans*, 119, 3834–3854,  
761 <https://doi.org/10.1002/2014JC009803>, 2014.
- 762 Tzortziou, M., Herman, J. R., Cede, A., Loughner, C. P., Abuhassan, N., and Naik, S.: Spatial and temporal variability  
763 of ozone and nitrogen dioxide over a major urban estuarine ecosystem, *J Atmos Chem*, 72, 287–309,  
764 <https://doi.org/10.1007/s10874-013-9255-8>, 2013.
- 765 United Nations Conference on Trade and Development: COVID-19 and Maritime Transport Impact and Responses:  
766 [https://unctad.org/system/files/official-document/dtltblinf2020d1\\_en.pdf](https://unctad.org/system/files/official-document/dtltblinf2020d1_en.pdf), last access: 9 June 2021.
- 767 USEPA Facility Level GHG Emissions Data: <http://ghgdata.epa.gov/ghgp/main.do>, last access: 6 May 2021.



- 768 USEPA: Integrated Science Assessment (ISA) for Nitrogen Dioxide - Health Criteria:  
769 <https://www.epa.gov/isa/integrated-science-assessment-isa-nitrogen-dioxide-health-criteria>, last access: 9  
770 July 2021.
- 771 USEPA 2017 National Emissions Inventory (NEI) Data: [https://www.epa.gov/air-emissions-inventories/2017-](https://www.epa.gov/air-emissions-inventories/2017-national-emissions-inventory-nei-data)  
772 [national-emissions-inventory-nei-data](https://www.epa.gov/air-emissions-inventories/2017-national-emissions-inventory-nei-data), last access: 9 July 2021.
- 773 Valin, L. C., Russell, A. R., and Cohen, R. C.: Variations of OH radical in an urban plume inferred from NO<sub>2</sub> column  
774 measurements, *Geophys. Res. Lett.*, 40, 1856–1860, <https://doi.org/10.1002/grl.50267>, 2013.
- 775 Veeffkind, J. P., Aben, I., McMullan, K., Förster, H., de Vries, J., Otter, G., Claas, J., Eskes, H. J., de Haan, J. F.,  
776 Kleipool, Q., van Weele, M., Hasekamp, O., Hoogeveen, R., Landgraf, J., Snel, R., Tol, P., Ingmann, P.,  
777 Voors, R., Kruizinga, B., Vink, R., Visser, H., and Levelt, P. F.: TROPOMI on the ESA Sentinel-5 Precursor:  
778 A GMES mission for global observations of the atmospheric composition for climate, air quality and ozone  
779 layer applications, *Remote Sensing of Environment*, 120, 70–83, <https://doi.org/10.1016/j.rse.2011.09.027>,  
780 2012.
- 781 Verhoelst, T., Compornolle, S., Pinardi, G., Lambert, J.-C., Eskes, H. J., Eichmann, K.-U., Fjæraa, A. M., Granville,  
782 J., Niemeijer, S., Cede, A., Tiefengraber, M., Hendrick, F., Pazmiño, A., Bais, A., Bazureau, A., Boersma,  
783 K. F., Bognar, K., Dehn, A., Donner, S., Elokhov, A., Gebetsberger, M., Goutail, F., Grutter de la Mora, M.,  
784 Gruzdev, A., Gratsea, M., Hansen, G. H., Irie, H., Jepsen, N., Kanaya, Y., Karagkiozidis, D., Kivi, R., Kreher,  
785 K., Levelt, P. F., Liu, C., Müller, M., Navarro Comas, M., Piters, A. J. M., Pommereau, J.-P., Portafaix, T.,  
786 Prados-Roman, C., Puentedura, O., Querel, R., Remmers, J., Richter, A., Rimmer, J., Rivera Cárdenas, C.,  
787 Saavedra de Miguel, L., Sinyakov, V. P., Stremme, W., Strong, K., Van Roozendaal, M., Veeffkind, J. P.,  
788 Wagner, T., Wittrock, F., Yela González, M., and Zehner, C.: Ground-based validation of the Copernicus  
789 Sentinel-5P TROPOMI NO<sub>2</sub> measurements with the NDACC ZSL-DOAS, MAX-DOAS and Pandonia  
790 global networks, *Atmos. Meas. Tech.*, 14, 481–510, <https://doi.org/10.5194/amt-14-481-2021>, 2021.
- 791 Verstraeten, W. W., Boersma, K. F., Douros, J., Williams, J. E., Eskes, H., Liu, F., Beirle, S., and Delcloo, A.: Top-  
792 Down NO<sub>x</sub> Emissions of European Cities Based on the Downwind Plume of Modelled and Space-Borne  
793 Tropospheric NO<sub>2</sub> Columns, *Sensors*, 18, 2893, <https://doi.org/10.3390/s18092893>, 2018.
- 794 WHO: Ten health issues WHO will tackle this year: [https://www.who.int/news-room/spotlight/ten-threats-to-global-](https://www.who.int/news-room/spotlight/ten-threats-to-global-health-in-2019)  
795 [health-in-2019](https://www.who.int/news-room/spotlight/ten-threats-to-global-health-in-2019), last access: 3 May 2021
- 796 Xu, W. Y., Zhao, C. S., Ran, L., Deng, Z. Z., Liu, P. F., Ma, N., Lin, W. L., Xu, X. B., Yan, P., He, X., Yu, J., Liang,  
797 W. D., and Chen, L. L.: Characteristics of pollutants and their correlation to meteorological conditions at a  
798 suburban site in the North China Plain, *Atmos. Chem. Phys.*, 11, 4353–4369, [https://doi.org/10.5194/acp-11-](https://doi.org/10.5194/acp-11-4353-2011)  
799 [4353-2011](https://doi.org/10.5194/acp-11-4353-2011), 2011.
- 800 Zhao, X., Griffin, D., Fioletov, V., McLinden, C., Cede, A., Tiefengraber, M., Müller, M., Bognar, K., Strong, K.,  
801 Boersma, F., Eskes, H., Davies, J., Ogyu, A., and Lee, S. C.: Assessment of the quality of TROPOMI high-  
802 spatial-resolution NO<sub>2</sub> data products in the Greater Toronto Area, *Atmos. Meas. Tech.*, 13, 2131–2159,  
803 <https://doi.org/10.5194/amt-13-2131-2020>, 2020.
- 804